https://ntrs.nasa.gov/search.jsp?R=19680007915 2018-07-21T08:51:27+00:00Z

NATIONAL AERONAUTICS AND SPACE ADMINISTRATION

Technical Report 32-1217

Behavior of Triangular Shell Element Stiffness Matrices Associated with Polyhedral Deflection Distributions

Senol Utku
Jet Propulsion Laboratory
Robert J. Melosh
Philco–Ford Corporation
Western Development Laboratories

N68-17384
(ACCESSION NUMBER)
25
(PAGES)
CR-93206
(NASA CR OR TMX OR AD NUMBER)
(THRU)
1
(CODE)
32
(CATEGORY)
FF No. 602(C)
~~AVAILABLE TO U.S. GOVERNMENT AGENCIES ONLY~~

JET PROPULSION LABORATORY
CALIFORNIA INSTITUTE OF TECHNOLOGY
PASADENA, CALIFORNIA

February 15, 1968

NATIONAL AERONAUTICS AND SPACE ADMINISTRATION

Technical Report 32-1217

Behavior of Triangular Shell Element Stiffness Matrices Associated with Polyhedral Deflection Distributions

Senol Utku
Jet Propulsion Laboratory
Robert J. Melosh
Philco–Ford Corporation
Western Development Laboratories

Approved by:

M. E. Alper

M. E. Alper, *Manager*
Applied Mechanics Section

JET PROPULSION LABORATORY
CALIFORNIA INSTITUTE OF TECHNOLOGY
PASADENA, CALIFORNIA

February 15, 1968

TECHNICAL REPORT 32-1217

Copyright © 1968
Jet Propulsion Laboratory
California Institute of Technology

Prepared Under Contract No. NAS 7-100
National Aeronautics & Space Administration

PRECEDING PAGE BLANK NOT FILMED.

Contents

I. Introduction 1

II. Review of Derivation 2

III. Close Examination of Element Stiffness Matrices 7

IV. Proposed Improvements 10

A. Absolute Value Scheme 11

B. Constant Trace Scheme 11

C. Average Rotations Algorithm 12

V. Comparison of Methods of Improvement 13

VI. Suggested Matrix and Convergence Characteristics 15

VII. Analysis Guidelines 18

VIII. How the Curvatures Are Accounted For 19

IX. Summary of Significant Developments 19

References 20

Figures

1. Triangulation on middle surface and a triangular curved element 2
2. Local and nodal coordinate systems 6
3. Variation of eigenvalues of membrane stiffness matrix (33) with geometry 8
4. Variation of eigenvalues of bending stiffness matrix (21) with geometry 8
5. Variation of eigenvalues of transverse shear stiffness matrix (28) with geometry 8
6. Variation of eigenvalues of total stiffness matrix (36) with geometry 8
7. Variation of eigenvalues of membrane stiffness matrix (32) with z_0 9
8. Variation of eigenvalues of total stiffness matrix (35) with z_0 . . . 9

Contents (contd)

Figures (contd)

9. Variation of eigenvalues of membrane stiffness matrix (30) with x_0 9

10. Variation of eigenvalues of total stiffness matrix (34) with x_0 9

11. Variation of eigenvalues of base shear matrix (26) with geometry 10

12. Variation of eigenvalues with geometry, after absolute value scheme 11

13. Variation of eigenvalues with geometry, after constant trace scheme 12

14. Variation of eigenvalues of transverse shear stiffness matrix (47) with geometry 13

15. Variation of eigenvalues of total stiffness matrix (48) with geometry 13

16. Effect of triangulation on the solution by (36) 14

17. Transverse displacements of centrally loaded clamped square plate along +x-axis 14

18. Transverse displacements of centrally loaded clamped square plate along x-axis 14

19. Comparison of convergence rates of equilibrium and average rotations algorithms 15

20. Clamped square plate subjected to a transverse concentrated force at center 16

21. Clamped spherical cap subjected to pressure loading 16

22. Clamped spherical cap subjected to a transverse concentrated force at center 17

23. Clamped spherical cap subjected to a transverse concentrated force at center 17

24. Demonstration of the fact that deflections vary basically with thickness cubed 18

25. Transverse displacement of centrally loaded clamped square plate 18

26. Advantage of using smaller mesh size around the concentrated load for rapid convergence 18

27. Effect of accuracy in nodal coordinates on the solution 19

Abstract

Invariants of the triangular shell element stiffness matrices are examined. The stiffness matrix is considered as the sum of membrane bending and transverse shear stiffness matrices representing respective strain energies. For various geometries and curvatures, eigenvalues of these matrices are obtained numerically. By studying the eigenvalues, it is shown that stiffness matrices produced with the help of equilibrium requirements may display nonpositive behavior depending upon element geometry. The grave consequences of nonpositive behavior are demonstrated. Since equilibrium algorithms can be used to accelerate the convergence, two schemes are developed to correct the nonpositive behavior. These schemes are based on the observation that nonpositive behavior originates from the base matrix to which equilibrium algorithm is applied. The effect of thickness/area ratio on the overall behavior is studied. The behavior associated with true potential energy approach is demonstrated on several test cases. The effect of geometry is also discussed in the assembled matrix. Guidelines have been presented for the use of the triangular shell element in structural analyses.

Behavior of Triangular Shell Element Stiffness Matrices Associated with Polyhedral Deflection Distributions*

I. Introduction

The finite element representations for thin structures have been developed parallel to the variety of the most used middle surface geometries. Axially symmetric finite elements for shells of revolution and polygonal finite elements for plates and shells of arbitrary geometry have been used. Rings, conical elements, and elements which are obtained by cutting the shell along its parallels have been considered for shells of revolution. Polygonal elements have been mostly either triangular or quadrilateral in shape, and generally proposed for stretching and/or bending of plates.

The deflection fields used during the derivation of elemental stiffness matrices show more diversity than the element shapes. For plates and shells of arbitrary geometry, mostly piecewise linear, quadratic and cubic fields have been considered. Since not all of these fields are admissible for the solution of extremum formulation of the equilibrium problems of thin structures, the detailed behaviors of many available representations are unknown, in addition to the fact that most of them are theoretically unacceptable.

Comparatively little work has been reported on the polygonal element representation of shells of arbitrary geometry for which elements with axial symmetry cannot be used. Melosh (Ref. 1) has presented a flat triangular element representation for plates and shells of arbitrary geometry. Utku (Ref. 2), starting from the shallow shell theory, developed stiffness matrices to include curvatures in the element. These matrices reduce to a slightly different version of the flat element stiffness matrix of Melosh when the curvatures in the element vanish. Since these authors have considered only polyhedral deflection distributions, the fields, being piecewise linear, are admissible for the solutions. However, a detailed examination of the behavior of these representations has not been made.

It is the purpose of this paper to review the basis of the triangular shell element representations given in Refs. 1 and 2, to examine their behavior by studying their intrinsic characteristics as a function of element geometry, and to illustrate the fact that solutions with the triangular shell element indeed yield a minimizing sequence for total

*This report was first presented at the AIAA 5th Aerospace Sciences Meeting, New York, January 1967, Paper 67-114.

potential energy (or a maximizing sequence for total strain energy) with grid refinement, and that the sequence is actually of the monotonically converging type.

The following section of this paper provides the derivation of the several stiffness matrices of triangular shell element. The third section examines the characteristics of these matrices as a function of the geometry of element. The fourth section evaluates means of improving the representations in case of nonpositive behavior. The fifth section correlates the theoretically developed conclusions with the effect of improvements in the solution problems. The sixth section discusses a best representation and illustrates, in some sample problems, the minimizing sequences for total potential energy as obtained with this element. The seventh section presents some guidelines the analyst should follow to use the triangular shell element to best advantage in numerical analyses. The eighth section discusses how curvatures are accounted for in the element representation. The final section summarizes the significant developments presented.

II. Review of Derivation

The derivation (Ref. 2) of the elemental stiffness matrices is summarized below. The triangulation of the middle surface and a triangular shell element are shown in Fig. 1. The right-handed coordinate system(xyz) is located at the centroid of base triangle 123 such that the x- and y-axes are coincident with its principal axes of moment of inertia, and the z-axis is such that an observer along it sees the node labels 1, 2, and 3 increasing in module 3 in the counterclockwise direction. The base triangle is obtained by joining the nodes 1, 2, and 3 with straight lines. Let U_M, U_B, and U_S represent membrane, bending, and transverse shear strain energies of the element. Then the elemental total strain energy U may be written as

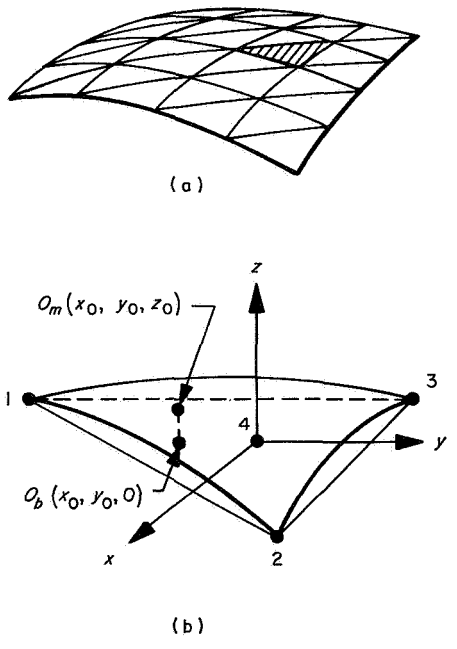

Fig. 1. Triangulation on middle surface and a triangular curved element

$$U = U_M + U_B + U_S \tag{1}$$

Designating the thickness as t, the area of the element as A, middle surface strains as $[\boldsymbol{\varepsilon}_0] = [\epsilon_{x0}\epsilon_{y0}\epsilon_{xy0}]$, changes in curvatures as $[\mathbf{X}] = [X_x X_y X_{xy}]$, transverse shear strains as $[\gamma] = [\gamma_{xz}\gamma_{yz}]$, and material matrices (3×3 and 2×2 matrices relating $[\boldsymbol{\varepsilon}_0]$ and $[\gamma]$ with the associated stresses) as $[\mathbf{D}]$ and $[\mathbf{D}']$, and using the Kirchhoff assumptions that no normal stress develops across thickness and strains on planes parallel to the tangent planes of middle surface vary linearly across thickness, one can write:

$$U_M = \frac{t}{2}\int_A [\boldsymbol{\varepsilon}_0][\mathbf{D}]\{\boldsymbol{\varepsilon}_0\}\, dA \tag{2}$$

$$U_B = \frac{t}{24}\int_A [\mathbf{X}][\mathbf{D}]\{\mathbf{X}\}\, dA \tag{3}$$

$$U_S = \frac{t}{2}\int_A [\gamma][\mathbf{D}']\{\gamma\}\, dA \tag{4}$$

In (4), it is assumed that $\{\gamma\}$ is constant across thickness.

Let $\mathbf{q}$ and $\boldsymbol{\theta}$ represent the displacement and the rotation vectors of middle surface points and normals at these points, respectively. The components of $\mathbf{q}$ and $\boldsymbol{\theta}$ are dedefined as

$$\mathbf{q} = u\mathbf{i} + v\mathbf{j} + w\mathbf{k} \tag{5}$$

$$\boldsymbol{\theta} = \theta_x\mathbf{i} + \theta_y\mathbf{j} \tag{6}$$

where $\mathbf{i}$, $\mathbf{j}$, and $\mathbf{k}$ are the unit vectors of coordinate axes. Expressing the undeformed middle surface with $z = z(x,y)$, and using the shallow shell theory (Ref. 3), one writes

$$\{\boldsymbol{\varepsilon}_0\} = \begin{Bmatrix} u_{,x} + z_{,x}w_{,x} \\ v_{,y} + z_{,y}w_{,y} \\ u_{,y} + v_{,x} + z_{,x}w_{,y} + z_{,y}w_{,x} \end{Bmatrix} \tag{7}$$

$$\{\mathbf{X}\} = \begin{Bmatrix} -\theta_{y,x} \\ \theta_{x,y} \\ \theta_{x,x} - \theta_{y,y} \end{Bmatrix} \tag{8}$$

$$\{\gamma\} = \begin{Bmatrix} w_{,x} \\ w_{,y} \end{Bmatrix} + \begin{Bmatrix} \theta_y \\ -\theta_x \end{Bmatrix} \tag{9}$$

(A comma in the subscript indicates partial differentiation with respect to the quantity or quantities following the comma.)

One can express U, approximately, by assuming an approximate deflection distribution in the triangular subdomain in terms of some undetermined parameters. In order to assure a maximizing sequence for U, with grid refinement on the middle surface, a polyhedral deflection distribution may be assumed (Ref. 4). This implies that the undetermined parameters are the nodal values of deflection components u, v, w, θ_x, and θ_y and that they vary linearly in any triangular subdomain.

$$\begin{Bmatrix} u \\ v \\ w \\ \theta_x \\ \theta_y \end{Bmatrix} \cong \frac{1}{2A} \begin{bmatrix} u_1 & u_2 & u_3 \\ v_1 & v_2 & v_3 \\ w_1 & w_2 & w_3 \\ \theta_{x1} & \theta_{x2} & \theta_{x3} \\ \theta_{y1} & \theta_{y2} & \theta_{y3} \end{bmatrix} \times \begin{bmatrix} y_{23} & x_{32} & r_1 \\ y_{31} & x_{13} & r_2 \\ y_{12} & x_{21} & r_3 \end{bmatrix} \begin{Bmatrix} x \\ y \\ 1 \end{Bmatrix} \tag{10}$$

where A is the area of the base triangle, u_i, v_i, w_i, θ_{xi}, and θ_{yi}, are the deflection components at the ith node, $x_{ij} = x_i - x_j$, $y_{ij} = y_i - y_j$, $r_i = x_{i+1}y_{i+2} - x_{i+2}y_{i+1}$ (subscripts are in module 3), and x and y are the coordinates of a point in the base triangle. Using (10) in (7), (8), and (9), one obtains

$$\{\boldsymbol{\varepsilon}_0\} \cong \frac{1}{2A} [\mathbf{M} \,\vdots\, \mathbf{N} \,\vdots\, z_{,x}\mathbf{M} + z_{,y}\mathbf{N}] \begin{Bmatrix} \mathbf{u} \\ \hdashline \mathbf{v} \\ \hdashline \mathbf{w} \end{Bmatrix} \tag{11}$$

$$\{\mathbf{X}\} \cong \frac{1}{2A} [-\mathbf{N} \,\vdots\, \mathbf{M}] \begin{Bmatrix} \boldsymbol{\theta}_x \\ \hdashline \boldsymbol{\theta}_y \end{Bmatrix} \tag{12}$$

$$\{\gamma\} \cong \frac{1}{2A}[\mathbf{L}][\mathbf{w}] + \begin{Bmatrix} \theta_y \\ \hdashline -\theta_x \end{Bmatrix} \tag{13}$$

where $[\mathbf{u}^T] = [u_1 u_2 u_3]$, $[\mathbf{v}^T] = [v_1 v_2 v_3]$, $[\mathbf{w}^T] = [w_1 w_2 w_3]$, $[\boldsymbol{\theta}_x{}^T] = [\theta_{x1}\theta_{x2}\theta_{x3}]$, $[\boldsymbol{\theta}_y^T] = [\theta_{y1}\theta_{y2}\theta_{y3}]$, dotted lines are partitioning lines, and

$$[\mathbf{M}] = \begin{bmatrix} y_{23} & y_{31} & y_{12} \\ 0 & 0 & 0 \\ x_{32} & x_{13} & x_{21} \end{bmatrix}$$

$$[\mathbf{N}] = \begin{bmatrix} 0 & 0 & 0 \\ x_{32} & x_{13} & x_{21} \\ y_{23} & y_{31} & y_{12} \end{bmatrix}$$

$$[\mathbf{L}] = \begin{bmatrix} y_{23} & y_{31} & y_{12} \\ x_{32} & x_{13} & x_{21} \end{bmatrix} \tag{14}$$

Assuming that the undeformed middle surface may be described approximately with a quadratic surface, one may write

$$z_{,x} = \alpha_1(x - x_0) + \alpha_2(y - y_0) \tag{15}$$

$$z_{,y} = \alpha_2(x - x_0) + \alpha_3(y - y_0) \tag{16}$$

where x_0 and y_0 are the coordinates of middle surface point O_M (Fig. 1b), whose tangent plane is parallel to the base triangle (z_0 is the z coordinate of this point), α_1 and α_3 are the average normal curvatures in the x and y directions, and α_2 is the average cross-curvature of the middle surface. Note that α_1, α_2 and α_3 can be uniquely defined if nodes 1, 2, 3 and point O_M are given.

Substituting (15) and (16) into (11), and (11), (12), and (13) into (2), (3), and (4), one obtains, after integration,

$$U_M = \frac{1}{2}[\mathbf{d}^T][\mathbf{K}_M]\{\mathbf{d}\} \tag{17}$$

$$U_B = \frac{1}{2}[\mathbf{d}^T][\mathbf{K}_B]\{\mathbf{d}\} \tag{18}$$

$$U_S = \frac{1}{2}[\mathbf{d}^T][\mathbf{K}_S]\{\mathbf{d}\} \tag{19}$$

where $[\mathbf{d}^T] = [\mathbf{u}^T\ \mathbf{v}^T\ \mathbf{w}^T\ \boldsymbol{\theta}_x^T\ \boldsymbol{\theta}_y^T]$, and $[\mathbf{K}_M]$, $[\mathbf{K}_B]$, and $[\mathbf{K}_S]$ are as follows

$$[\mathbf{K}_M] = \frac{t}{4A}\left[\begin{array}{c:c:c:c:c} \mathbf{P} & \mathbf{R} & \mathbf{F}_{11}^T & \mathbf{0} & \mathbf{0} \\ \hdashline \mathbf{R}^T & \mathbf{Q} & \mathbf{G}_{11}^T & \mathbf{0} & \mathbf{0} \\ \hdashline \mathbf{F}_{11} & \mathbf{G}_{11} & \mathbf{H}_{11} & \mathbf{0} & \mathbf{0} \\ \hdashline \mathbf{0} & \mathbf{0} & \mathbf{0} & \mathbf{0} & \mathbf{0} \\ \hdashline \mathbf{0} & \mathbf{0} & \mathbf{0} & \mathbf{0} & \mathbf{0} \end{array}\right] \tag{20}$$

$$[\mathbf{K}_B] = \frac{t^3}{48A}\left[\begin{array}{c:c:c:c:c} \mathbf{0} & \mathbf{0} & \mathbf{0} & \mathbf{0} & \mathbf{0} \\ \hdashline \mathbf{0} & \mathbf{0} & \mathbf{0} & \mathbf{0} & \mathbf{0} \\ \hdashline \mathbf{0} & \mathbf{0} & \mathbf{0} & \mathbf{0} & \mathbf{0} \\ \hdashline \mathbf{0} & \mathbf{0} & \mathbf{0} & \mathbf{Q} & -\mathbf{R}^T \\ \hdashline \mathbf{0} & \mathbf{0} & \mathbf{0} & -\mathbf{R} & \mathbf{P} \end{array}\right] \tag{21}$$

$$[\mathbf{K}_S] = \frac{t}{4A}\left[\begin{array}{c:c:c:c:c} \mathbf{0} & \mathbf{0} & \mathbf{0} & \mathbf{0} & \mathbf{0} \\ \hdashline \mathbf{0} & \mathbf{0} & \mathbf{0} & \mathbf{0} & \mathbf{0} \\ \hdashline \mathbf{0} & \mathbf{0} & \mathbf{S}_{11} & \mathbf{W}_{21}^T & \mathbf{W}_{31}^T \\ \hdashline \mathbf{0} & \mathbf{0} & \mathbf{W}_{21} & d'_{22}\mathbf{W} & -d'_{21}\mathbf{W} \\ \hdashline \mathbf{0} & \mathbf{0} & \mathbf{W}_{31} & -d'_{21}\mathbf{W} & d'_{11}\mathbf{W} \end{array}\right] \tag{22}$$

where

$$\begin{aligned} [\mathbf{P}] &= [\mathbf{M}^T][\mathbf{D}][\mathbf{M}] \\ [\mathbf{R}] &= [\mathbf{M}^T][\mathbf{D}][\mathbf{N}] \\ [\mathbf{Q}] &= [\mathbf{N}^T][\mathbf{D}][\mathbf{N}] \end{aligned} \tag{23a}$$

$$\begin{aligned} [\mathbf{F}_{11}] &= a[\mathbf{P}] + b[\mathbf{R}^T] \\ [\mathbf{G}_{11}] &= a[\mathbf{R}] + b[\mathbf{Q}] \\ [\mathbf{H}_{11}] &= c[\mathbf{P}] + d[\mathbf{Q}] + e([\mathbf{R}] + [\mathbf{R}^T]) \end{aligned} \tag{23b}$$

$$\begin{aligned} [\mathbf{S}_{11}] &= [\mathbf{L}^T][\mathbf{D}'][\mathbf{L}] \\ [\mathbf{W}_{21}] &= -\begin{bmatrix} 0 & 0 \\ 0 & 0 \\ d'_{21} & d'_{22} \end{bmatrix}[\mathbf{L}] \\ [\mathbf{W}_{31}] &= \begin{bmatrix} 0 & 0 \\ 0 & 0 \\ d'_{11} & d'_{21} \end{bmatrix}[\mathbf{L}] \\ [\mathbf{W}] &= \begin{bmatrix} I_y/A & 0 & 0 \\ 0 & I_x/A & 0 \\ 0 & 0 & 1 \end{bmatrix} \end{aligned} \tag{23c}$$

and

$$\begin{aligned} a &= -x_0\alpha_1 - y_0\alpha_2 \\ b &= -x_0\alpha_2 - y_0\alpha_3 \\ c &= (x_0^2 + I_y/A)\alpha_1^2 + (y_0^2 + I_x/A)\alpha_2^2 \\ &\quad + x_0y_0\alpha_1\alpha_2 \\ d &= (y_0^2 + I_x/A)\alpha_3^2 + (x_0^2 + I_y/A)\alpha_2^2 \\ &\quad + x_0y_0\alpha_2\alpha_3 \\ e &= (x_0^2 + I_y/A)\alpha_1\alpha_2 + (y_0^2 + I_x/A)\alpha_2\alpha_3 \\ &\quad + x_0y_0(\alpha_1\alpha_3 + \alpha_2^2) \end{aligned} \tag{24}$$

where $[\mathbf{0}]$ represents the zero matrix of order 3, I_x and I_y are the principal moments of inertia of the base triangle, and d'_{11}, d'_{21}, and d'_{22} are the elements of $[\mathbf{D}']$.

Since the second deflection derivatives of U give the elemental stiffness matrix, one can write

$$[\mathbf{K}] = [\mathbf{K}_M] + [\mathbf{K}_B] + [\mathbf{K}_S] \tag{25}$$

where $[\mathbf{K}_M]$, $[\mathbf{K}_B]$, and $[\mathbf{K}_S]$ are elemental membrane, bending, and transverse shear stiffness matrices and are defined by (20), (21), and (22).

It has been demonstrated (Ref. 1) that $[\mathbf{K}_S]$ causes a maximizing sequence of extremely slow convergence with grid refinement, and the columns of $[\mathbf{K}_M]$, in general, only approximately satisfy the moment equilibrium requirements (Ref. 2), although the force equilibrium requirements are satisfied exactly. (This can be seen readily from (14) and (23) by noting that row sums of $[\mathbf{M}]$ and $[\mathbf{N}]$, and, consequently, $[\mathbf{P}]$, $[\mathbf{Q}]$, and $[\mathbf{R}]$, are zero.)

The undesirable behavior of $[\mathbf{K}_S]$ originates from the fact that the linear variation of w is not compatible with the linear variations of θ_x and θ_y for large grid sizes. To accelerate the convergence it has been proposed (Ref. 1) to replace (22) with the sum of transverse shear stiffness matrices of hypothetical spar beams at the periphery of the element, the rigidities of which are adjusted such that when the base triangle is a right triangle the third submatrix on the diagonal becomes identical with that of (22). This proposal will be examined closely in Section IV.

Another proposal (Ref. 2) for rapid convergence is to ignore the contributions of θ_x and θ_y to $\{\gamma\}$ in (13) before integrating and differentiating U_S, (4), which leads to

$$[\mathbf{K}'_{S1}] = \frac{t}{4A}\left[\begin{array}{c|c|c|c|c} \mathbf{0} & \mathbf{0} & \mathbf{0} & \mathbf{0} & \mathbf{0} \\ \hline \mathbf{0} & \mathbf{0} & \mathbf{0} & \mathbf{0} & \mathbf{0} \\ \hline \mathbf{0} & \mathbf{0} & \mathbf{S}_{11} & \mathbf{0} & \mathbf{0} \\ \hline \mathbf{0} & \mathbf{0} & \mathbf{0} & \mathbf{0} & \mathbf{0} \\ \hline \mathbf{0} & \mathbf{0} & \mathbf{0} & \mathbf{0} & \mathbf{0} \end{array}\right] \tag{26}$$

where

$$[\mathbf{S}_{11}] = [\mathbf{L}^T][\mathbf{D}'][\mathbf{L}] \tag{27}$$

Since row sums of $[\mathbf{L}]$ are zero (see 14), the row sums of $[\mathbf{S}_{11}]$ are also zero, which implies that the columns of $[\mathbf{K}'_{S1}]$ satisfy the force equilibrium requirements. However, they do not satisfy the moment equilibrium requirements. The contributions of θ_x and θ_y may now be taken into account to satisfy the moment equilibrium requirements. This can be achieved by computing the unbalanced moments for each column of (26), starting from the 7th, and then distributing as suggested in Ref. (2), using the procedure called "equilibrium algorithm." This procedure leads to

$$[\mathbf{K}_{S1}] = \frac{t}{4A}\left[\begin{array}{c|c|c|c|c} \mathbf{0} & \mathbf{0} & \mathbf{0} & \mathbf{0} & \mathbf{0} \\ \hline \mathbf{0} & \mathbf{0} & \mathbf{0} & \mathbf{0} & \mathbf{0} \\ \hline \mathbf{0} & \mathbf{0} & \mathbf{S}_{11} & \mathbf{S}_{21}^T & \mathbf{S}_{31}^T \\ \hline \mathbf{0} & \mathbf{0} & \mathbf{S}_{21} & \mathbf{S}_{22} & \mathbf{S}_{32}^T \\ \hline \mathbf{0} & \mathbf{0} & \mathbf{S}_{31} & \mathbf{S}_{32} & \mathbf{S}_{33} \end{array}\right] \tag{28}$$

The explicit expressions for the elements of $[\mathbf{S}_{ij}]$ submatrices may be obtained as follows. Let $[\mathbf{f}]$, $[\mathbf{m}_x]$, and $[\mathbf{m}_y]$ stand for the third, the fourth, and the fifth submatrices, respectively, of any column of (28). The elements of $[\mathbf{m}_x]$ and $[\mathbf{m}_y]$ may be expressed explicitly as

$$m_{xij} = -\frac{1}{2}[(1-\delta_{ij})(f_{ij}y_{ij}) + \delta_{ij}(f_{i+1,j}y_{i+1,j} + f_{i+2,j}y_{i+2,j})] \tag{29a}$$

$$m_{yij} = \frac{1}{2}[(1-\delta_{ij})(f_{ij}x_{ij}) + \delta_{ij}(f_{i+1,j}x_{i+1,j} + f_{1+2,j}x_{i+2,j})] \tag{29b}$$

where the range of i and j is from 1 to 3, subscripts may take integer values of module 3, and δ_{ij} is the Kronecker delta. Matrix $[\mathbf{K}_{S1}]$ as given by (28) and (29) does satisfy force and moment equilibrium requirements, and it may be used in place of (22) for rapid convergence.

The difficulty arising from the fact that the moment equilibrium requirements in (20) are satisfied only approximately may be resolved, considering the coupling between membrane action and bending, in one of the following ways:

1. The equilibrium algorithm as described by (29) may be applied to the columns of (20), starting from the first and always assuming that $[\mathbf{f}]$ in (29) stands for the third row submatrices. This leads to:

$$[\mathbf{K}_{M1}] = \left[\begin{array}{c|c|c|c|c} \mathbf{P} & \mathbf{R} & \mathbf{F}_{11}^T & \mathbf{F}_{21}^T & \mathbf{F}_{31}^T \\ \hline \mathbf{R}^T & \mathbf{Q} & \mathbf{G}_{11}^T & \mathbf{G}_{21}^T & \mathbf{G}_{31}^T \\ \hline \mathbf{F}_{11} & \mathbf{G}_{11} & \mathbf{H}_{11} & \mathbf{H}_{21}^T & \mathbf{H}_{31}^T \\ \hline \mathbf{F}_{21} & \mathbf{G}_{21} & \mathbf{H}_{21} & \mathbf{H}_{22} & \mathbf{H}_{32}^T \\ \hline \mathbf{F}_{31} & \mathbf{G}_{31} & \mathbf{H}_{31} & \mathbf{H}_{32} & \mathbf{H}_{33} \end{array}\right] \tag{30}$$

This matrix satisfies both force and moment equilibrium requirements, with the exception of the moment equilibrium requirement about the z-axis, which is satisfied only approximately.

2. The middle surface may be approximated by a quadratic surface such that $x_0 = y_0 = 0$. Using $x_0 = y_0 = 0$ in (24), one obtains

$$
\begin{aligned}
a &= 0 \\
b &= 0 \\
c_0 &= \frac{(I_y\alpha_1^2 + I_x\alpha_2^2)}{A} \\
d_0 &= \frac{(I_x\alpha_3^2 + I_y\alpha_2^2)}{A} \\
e_0 &= \frac{(I_y\alpha_1 + I_x\alpha_3)\alpha_2}{A}
\end{aligned}
\tag{31}
$$

Substituting (31) in (30), one obtains

$$
[\mathbf{K}_{M2}] = \frac{t}{4A}\left[\begin{array}{c|c|c|c|c}
\mathbf{P} & \mathbf{R} & \mathbf{0} & \mathbf{0} & \mathbf{0} \\ \hline
\mathbf{R}^T & \mathbf{Q} & \mathbf{0} & \mathbf{0} & \mathbf{0} \\ \hline
\mathbf{0} & \mathbf{0} & \mathbf{B}_{11} & \mathbf{B}_{21}^T & \mathbf{B}_{31}^T \\ \hline
\mathbf{0} & \mathbf{0} & \mathbf{B}_{21} & \mathbf{B}_{22} & \mathbf{B}_{32}^T \\ \hline
\mathbf{0} & \mathbf{0} & \mathbf{B}_{31} & \mathbf{B}_{32} & \mathbf{B}_{33}
\end{array}\right]
\tag{32a}
$$

where

$$
[\mathbf{B}_{11}] = c_0[\mathbf{P}] + d_0[\mathbf{Q}] + e_0([\mathbf{R}] + [\mathbf{R}^T])
\tag{32b}
$$

Equations (32) satisfy both force and moment equilibrium requirements.

3. Observing that c_0, d_0, and e_0 are quantities proportional with $(\alpha r)^2$, where α designates average curvature and r is the radius of gyration of the base triangle, one may conclude that the contribution of the coupling between membrane action and bending will vanish rapidly with grid refinement. Therefore, for all practical purposes, this contribution might be ignored. Taking $c_0 = d_0 = e_0 = 0$ in (32), one obtains

$$
[\mathbf{K}_{M3}] = \frac{t}{4A}\left[\begin{array}{c|c|c|c|c}
\mathbf{P} & \mathbf{R} & \mathbf{0} & \mathbf{0} & \mathbf{0} \\ \hline
\mathbf{R}^T & \mathbf{Q} & \mathbf{0} & \mathbf{0} & \mathbf{0} \\ \hline
\mathbf{0} & \mathbf{0} & \mathbf{0} & \mathbf{0} & \mathbf{0} \\ \hline
\mathbf{0} & \mathbf{0} & \mathbf{0} & \mathbf{0} & \mathbf{0} \\ \hline
\mathbf{0} & \mathbf{0} & \mathbf{0} & \mathbf{0} & \mathbf{0}
\end{array}\right]
\tag{33}
$$

This matrix satisfies both force and moment equilibrium requirements and is the flat element membrane stiffness matrix.

Having derived various stiffness matrices for the triangular element, the total stiffness matrices may be written as the sum of membrane, bending, and transverse shear stiffness matrices. These are as follows:

For the general curved element with membrane-bending coupling:

$$
[\mathbf{K}_1] = [\mathbf{K}_{M1}] + [\mathbf{K}_B] + [\mathbf{K}_{S1}]
\tag{34}
$$

For the special curved element with membrane-bending coupling:

$$
[\mathbf{K}_2] = [\mathbf{K}_{M2}] + [\mathbf{K}_B] + [\mathbf{K}_{S1}]
\tag{35}
$$

For the flat element:

$$
[\mathbf{K}_3] = [\mathbf{K}_{M3}] + [\mathbf{K}_B] + [\mathbf{K}_{S1}]
\tag{36}
$$

Eq. (36) is the same as the equation given in Ref. (1), with some differences which will be discussed in Section IV. All these matrices are symmetric and satisfy both force and moment equilibrium requirements. They are examined closely in Section III.

The curvatures of the middle surface are really taken into account at the time of assembling the stiffness matrices of the neighboring elements. Just before assembly, each elemental stiffness matrix is expressed in a common coordinate system, which may differ from node to node. An element, its local coordinate system, and the coordinate systems at the nodes are shown in Fig. 2.

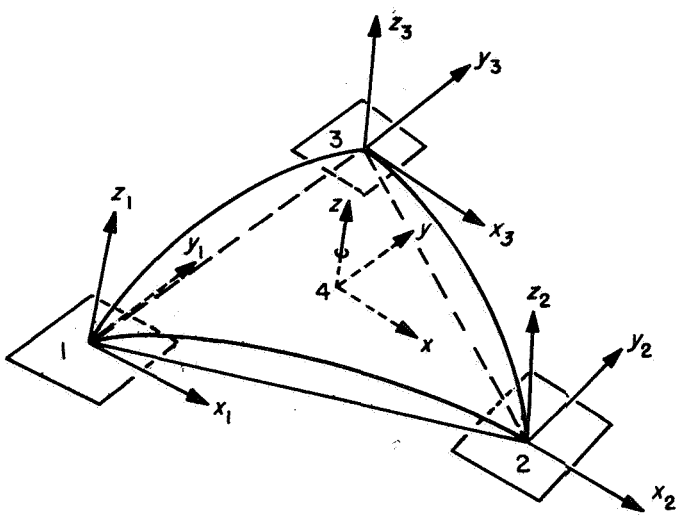

Fig. 2. Local and nodal coordinate systems

Expressing the nodal deflections and forces in the nodal coordinate systems, the elemental stiffness matrix in nodal coordinate systems becomes

$$[\mathbf{K}_c] = [\mathbf{Q}^T][\mathbf{K}][\mathbf{Q}] \tag{37}$$

where $[\mathbf{K}]$ designates $[\mathbf{K}_i]$, $i = 1, 2, 3$, and $[\mathbf{Q}]$ is the coordinate transformation matrix which contains the direction cosines of nodal coordinate axes in the local coordinate system. The direction cosines, when coupled with the distances between the nodes, implicitly express the average normal and geodesic curvatures of the middle surface. When the stiffness matrices of each element on the shell are expressed as (37), they can be assembled directly, as if they are the elemental stiffness matrices of a plate expressed in an overall coordinate system. In Section VIII, the manner in which the curvatures are handled is discussed further.

III. Close Examination of Element Stiffness Matrices

Not all of the matrices given in the previous section are direct results of the Ritz procedure with linear deflection fields. Several times, certain deflection components have been deliberately excluded from strain energy expressions for rapid convergence. When the stiffness matrices were so obtained, the condition that the columns should satisfy the force and moment equilibrium requirements was used to compensate the deliberate exclusions. The equilibrium condition is a practically important one; e.g., an overall stiffness matrix associated with a free-free structure and composed of elemental matrices violating the equilibrium requirements will have nonzero vibration frequencies for rigid body modes. Although the equilibrium device looks attractive, it may remove the positiveness of the problem as the elemental geometry changes. It is this point that justly motivated the close examination of the elemental stiffness matrices of the previous section.

The matrices presented in the previous section are all symmetric and satisfy the equilibrium requirements. Let $[\mathbf{K}]$ represent any of these matrices and U represent the strain energy associated with this matrix. Then

$$U = \frac{1}{2}\,[\mathbf{d}^T][\mathbf{K}]\{\mathbf{d}\} \tag{38}$$

where $\{\mathbf{d}\}$ is of order 15 and is as defined previously. Since $[\mathbf{K}]$ is real and symmetric, it can be diagonalized.

$$[\mathbf{K}] = [\mathbf{X}]^T[\lambda][\mathbf{X}] \tag{39}$$

where $[\lambda]$ is the diagonal matrix of eigenvalues and $[\mathbf{X}]$ is the matrix of associated eigenvectors.

Substituting (39) into (38),

$$U = \frac{1}{2}\,[\mathbf{d}^T][\mathbf{X}]^T[\lambda][\mathbf{X}]\{\mathbf{d}\} \tag{40}$$

and defining

$$\{\mathbf{q}\} = [\mathbf{X}]\{\mathbf{d}\} \tag{41}$$

as generalized deflections, one finally obtains

$$U = \frac{1}{2}\,[\mathbf{q}^T][\lambda]\{\mathbf{q}\} \tag{42}$$

Being energy, U is a positive quantity. Therefore, the diagonal matrix $[\lambda]$ can only have positive and zero diagonal elements. Negative values in the diagonal are the signs of nonpositive behavior. A discretization which causes nonpositive representations is dangerous as well as theoretically unsound. Negative eigenvalues will cause absurd results when the associated eigenvectors are excited by the loads. Since the columns of $[\mathbf{K}]$ satisfy, in general, five equilibrium conditions (the sixth condition, the moment equilibrium about the z-axis, is not important in the linear thin shell theory), the rank of $[\mathbf{K}]$, and consequently that of $[\lambda]$, cannot be larger than ten $(15 - 5 = 10)$. This implies that at least five boundary conditions should be imposed on $[\mathbf{K}]$ in order to make it positive definite (the case when all of the diagonal elements of the $[\lambda]$ are positive).

In order to find out if the use of the equilibrium condition could remove the positiveness of $\mathbf{K}$ matrices derived previously with changing geometry, a base triangle with nodal coordinates (0, 0, 0), (0, 4, 0) and $(x_3, 4, 0)$, for the first, second, and third nodes, respectively, in an (xyz) system located at node 1, is considered. The associated triangular shell element is assumed to be of thickness $t = 1$ in. and to be made of an homogeneous isotropic material of Young's modulus 10.67 10^6 psi and Poisson's ratio of 1/3. Point O_M of the middle surface (see Fig. 1b) is assumed to have coordinates x_0, y_0, and z_0 in the local coordinate system of the element (i.e., the system at the centroid of the base triangle).

For various values of x_3, x_0, and z_0, the matrices given by (33), (21), (28), (36), (32), (35), (30), (34), and (26) are

numerically diagonalized by means of successive rotations. The results are presented in Figs. 3 to 10. The study of these figures indicates the following:

(1) Flat or curved bending stiffness matrix (21) is always positive and of rank 3 regardless of the shape of the base triangle (Fig. 4).

(2) Flat element membrane stiffness matrix (33) is always positive and of rank 3 regardless of the shape of the base triangle (Fig. 3).

(3) Flat or curved element transverse shear stiffness matrix (28) and flat element total stiffness matrix (36) are positive if the triangle is not obtuse. The

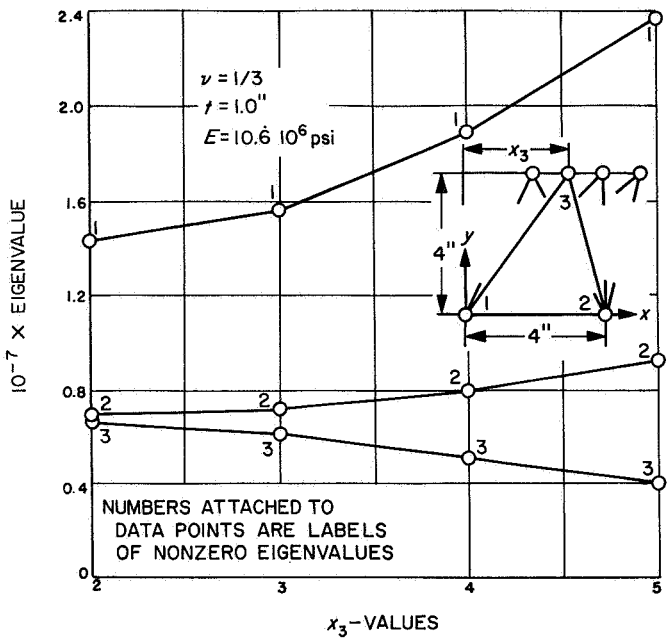

Fig. 3. Variation of eigenvalues of membrane stiffness matrix (33) with geometry ($x_0 = y_0 = z_0 = 0$)

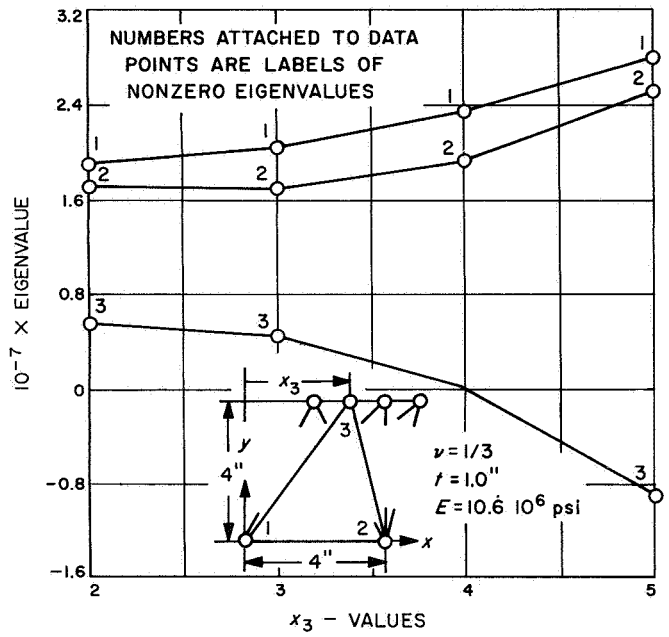

Fig. 5. Variation of eigenvalues of transverse shear stiffness matrix (28) with geometry

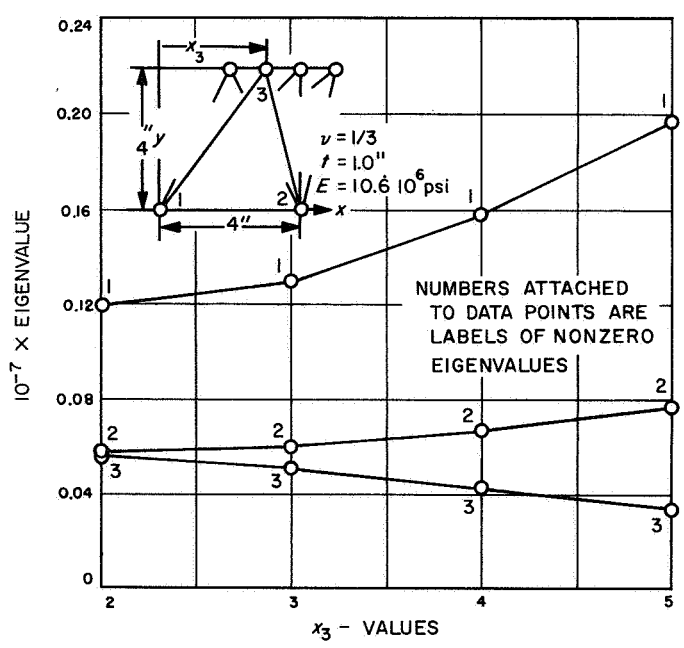

Fig. 4. Variation of eigenvalues of bending stiffness matrix (21) with geometry

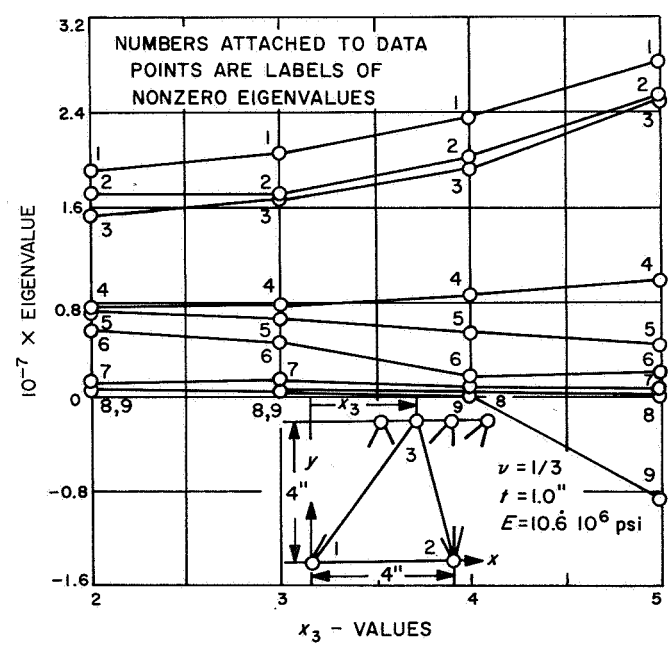

Fig. 6. Variation of eigenvalues of total stiffness matrix (36) with geometry

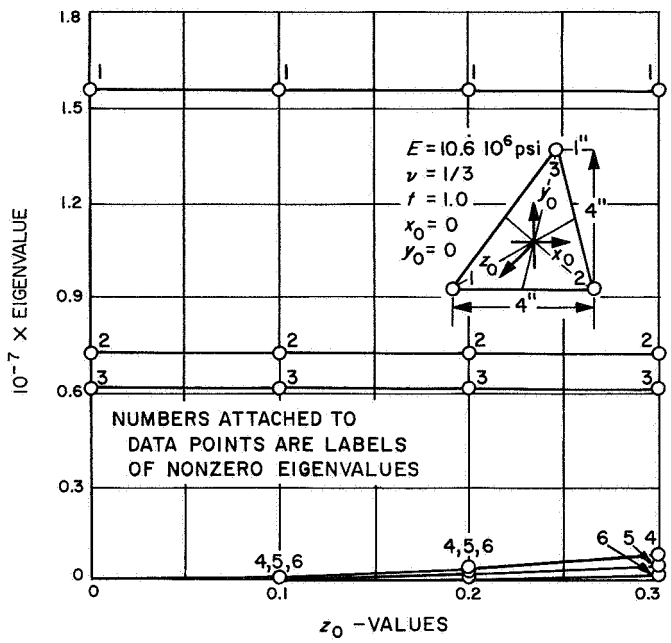

Fig. 7. Variation of eigenvalues of membrane stiffness matrix (32) with z_0($x_0 = y_0 = 0$ and triangle is not obtuse)

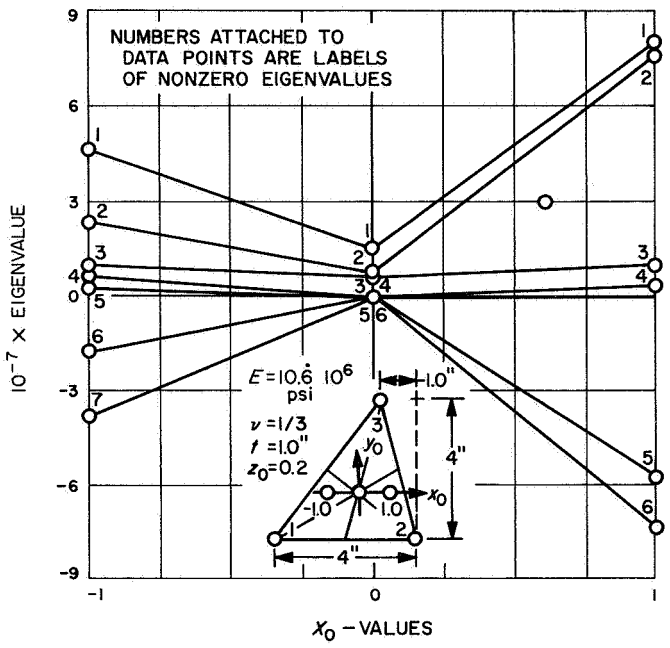

Fig. 9. Variation of eigenvalues of membrane stiffness matrix (30) with x_0($y_0 = 0$, z_0 prescribed, and triangle is not obtuse)

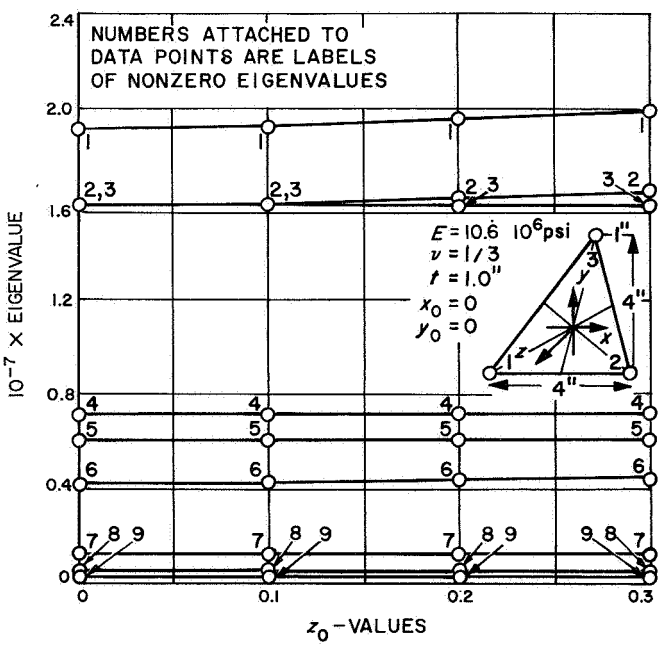

Fig. 8. Variation of eigenvalues of total stiffness matrix (35) with z_0($x_0 = y_0 = 0$ and triangle is not obtuse)

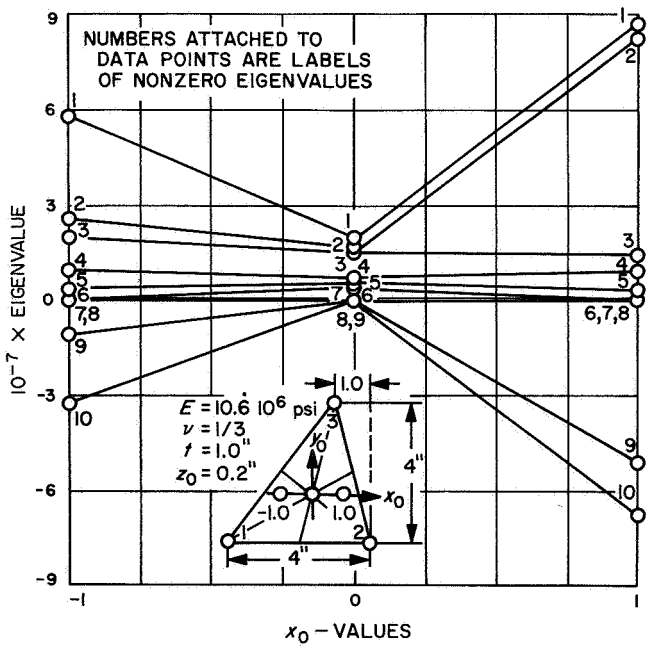

Fig. 10. Variation of eigenvalues of total stiffness matrix (34) with x_0($y_0 = 0$, z_0 prescribed, and triangle is not obtuse)

rank is 3 in (28) and 9 in (36) if the triangle is not a right triangle, in which case (28) is of rank 2 and (36) is of rank 8 (Figs. 5 and 6).

(4) Special curved element membrane stiffness matrix (32) and total matrix (35) are always positive when the triangle is not obtuse; (32) is of rank 6 and (35) is of rank 9 (Figs. 7 and 8).

(5) General curved element membrane and total stiffness matrices (30) and (34) are not positive unless $x_0 = y_0 = 0$ (Figs. 9 and 10).

(6) Shear stiffness matrix (26) is always positive and of rank 2, regardless of the shape of the base triangle (see Fig. 11).

The following is common for all cases:

(1) The spectrum width of eigenvalues (i.e., the difference between the highest and lowest eigenvalues) increases as the base triangle changes from isosceles to obtuse triangle.

(2) The spectrum width of eigenvalues increases with increasing average curvatures (i.e., with z_0).

(3) The spectrum width of eigenvalues increases with the distance from O_B to centroid (Fig. 1b).

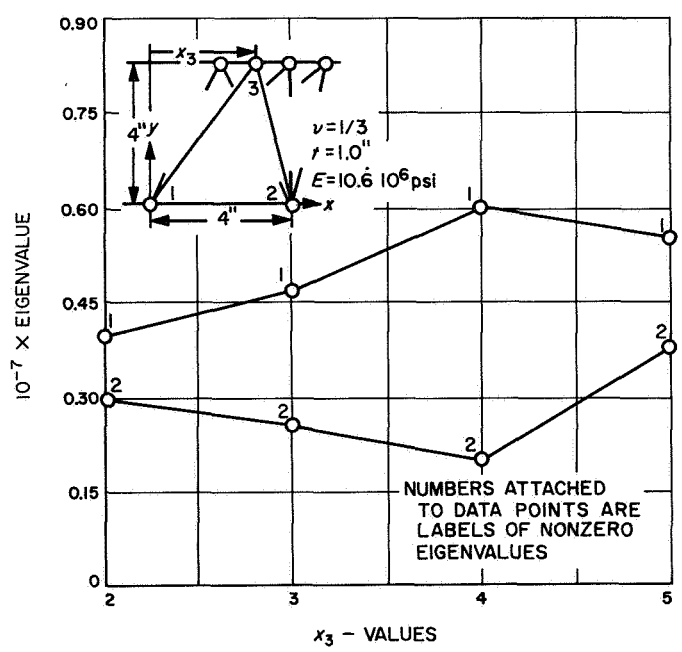

Fig. 11. Variation of eigenvalues of base shear matrix (26) with geometry

(4) Eigenvalues associated with bending modes are about one order of magnitude smaller than those associated with pure stretching and transverse shear modes.

This study clearly indicates that matrices which are obtained directly by piecewise linear fields are positive regardless of the geometry. However, those obtained with the help of the equilibrium algorithm may not be positive as the geometry changes.

Further investigations indicated that, rather than the equilibrium algorithm per se, the base matrix, e.g., $[\mathbf{S}_{11}]$ in (28), to which the equilibrium algorithm is applied is the starting point of the nonpositive behavior. It is observed that the equilibrium algorithm, when applied to base matrices with positive diagonal and nonpositive off-diagonal elements, always yields positive matrices. However when an off-diagonal element in the base matrix becomes positive, the equilibrium algorithm produces a nonpositive matrix. It can be shown that $[\mathbf{S}_{11}]$ in (28) will always have a positive off-diagonal element when the triangle is obtuse.

IV. Proposed Improvements

The examination of the eigenvalues has shown that the stiffness matrices which are developed with the help of equilibrium conditions may display nonpositive behavior depending upon the geometry. Transverse shear stiffness matrix (28) is not positive when the base triangle is obtuse, and the general curved element membrane matrix (30) is positive only if $x_0 = y_0 = 0$. A representation, which may yield a nonpositive matrix, is not satisfactory.

In Section III, it was indicated that the nonpositive behavior originates from the base matrix (e.g., $[\mathbf{S}_{11}]$, $[\mathbf{F}_{11}]$, $[\mathbf{G}_{11}]$, $[\mathbf{H}_{11}]$) to which the equilibrium algorithm is applied. Actually, these base matrices are obtained directly by integrating and then differentiating the strain energy expressions. Unless these base matrices are modified somehow, there is no way of preventing the above-mentioned nonpositive behaviors, if one is to use the equilibrium algorithm. Of course, there is always the possibility of discarding these nonpositive behaviors by careful triangulation of the middle surface.

In this section, two methods of improvement for the base matrix, the absolute value scheme and the constant trace scheme, are proposed to insure safe computation even in casually chosen grid configurations. These schemes involve arbitrary modification of base matrices when a

positive off-diagonal is encountered. Since very low energy is associated with the matrices generated from the base matrices, such modifications are justified. Later in the section, another method, the average rotations algorithm, is proposed, in which the coupling between membrane action and bending is ignored and the transverse shear stiffness matrix is generated without the help of equilibrium algorithm. These methods are described below.

A. Absolute Value Scheme

A well-behaved base matrix is in the following form:

$$[\mathbf{B}'] = \begin{bmatrix} a+b & -a & -b \\ -a & a+c & -c \\ -b & -c & b+c \end{bmatrix} \tag{43}$$

where a, b, and c are nonnegative. If the equilibrium algorithm is applied to this base matrix, it produces a positive matrix. Matrix (43) is the form of $[\mathbf{S}_{11}]$ when the triangle is not obtuse. It causes nonpositiveness if one of the off-diagonal elements is positive:

$$[\mathbf{B}''] = \begin{bmatrix} a+(-b) & -a & -(-b) \\ -a & a+c & -c \\ -(-b) & -c & (-b)+c \end{bmatrix} \tag{44}$$

which is the form of $[\mathbf{S}_{11}]$ when the triangle is obtuse. The absolute value scheme simply is to change the sign of the positive off-diagonal element to negative, i.e., to replace $-(-b)$ with $-(\,|-b|\,)$. When applied to (44), this scheme yields (43). Note that the scheme produces (43), if applied to (43).

The absolute value scheme arbitrarily alters material orthotropy or curvatures, depending upon whether the base matrix represents shear or membrane action. However, it is justified because of the low energy associated with respective matrices. Figure 12 shows the behaviors of transverse shear stiffness matrix (28) and the flat element stiffness matrix (36), respectively, after the absolute value scheme. Comparing this figure with Figs. 5 and 6, one observes that no negative eigenvalues develop in this scheme.

By taking the absolute values of the spar beam areas, Melosh (Ref. 1) has used this scheme in his triangular

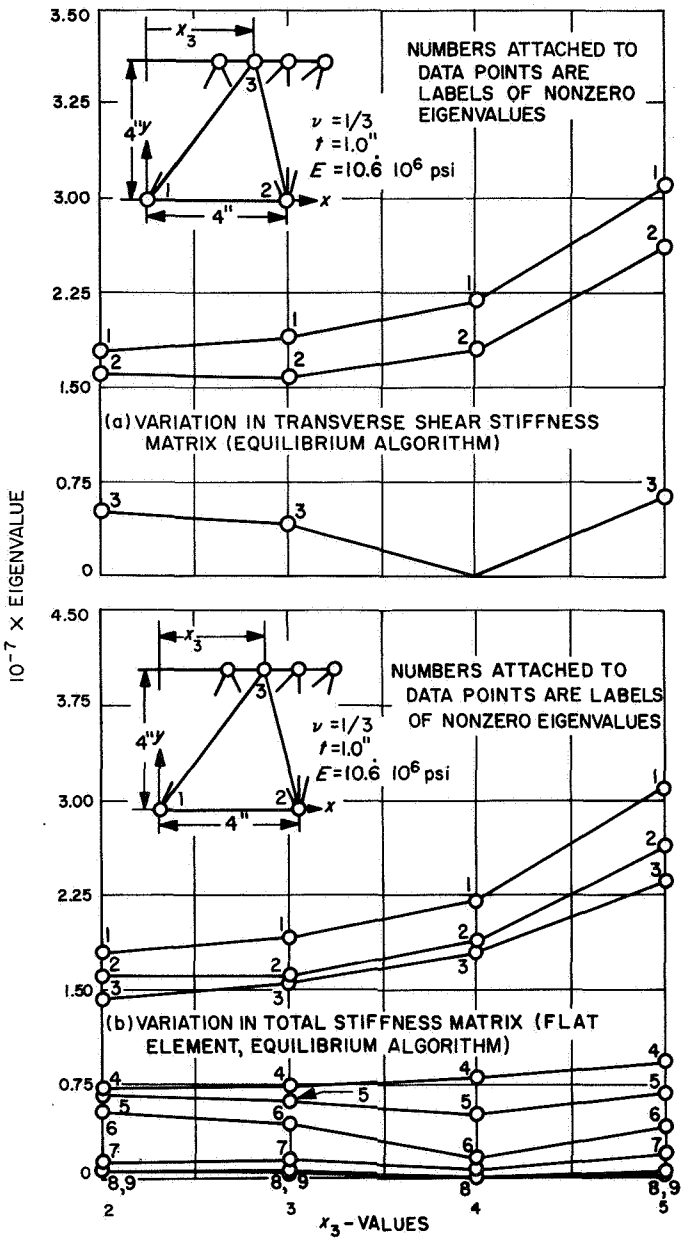

Fig. 12. Variation of eigenvalues with geometry, after absolute value scheme: (a) Transverse shear stiffness matrix (28); (b) Total stiffness matrix (36) ($x_0 = y_0 = z_0 = 0$)

facet element. If the absolute value signs are removed, Eqs. (7) and (8) of Ref. 1 are identical with (28).

B. Constant Trace Scheme

This scheme, when a positive off-diagonal exists, alters the base matrix such that its trace does not change. It consists of nullifying the positive off-diagonal element and

adjusting the others accordingly. When applied to (44), it yields:

$$[\mathbf{B}''] = \begin{bmatrix} a - \frac{b}{2} & -a + \frac{b}{2} & 0 \\ -a + \frac{b}{2} & a + c - b & -c + \frac{b}{2} \\ 0 & -c + \frac{b}{2} & c - \frac{b}{2} \end{bmatrix} \quad (45)$$

Note that the traces of (44) and (45) are both equal to $2a + 2c - 2b$.

This scheme, like the absolute value scheme, arbitrarily changes material orthotropies and element curvatures. However, it is justified because of the low energy associated with the respective matrices. Figures 13a and 13b show the behaviors of transverse shear matrix (28) and the flat element total stiffness matrix (36), respectively, after the constant trace scheme. Comparing these figures with Figs. 5 and 6, one observes that no negative eigenvalue develops in this scheme.

C. Average Rotations Algorithm

The algorithm presented here is an attempt to generate the transverse shear stiffness matrix without the help of equilibrium conditions. The advantage envisioned is the elimination of the arbitrariness involved in the absolute value and the constant trace schemes. It will be shown in the next section that this algorithm, although theoretically more sound, has poorer convergence characteristics than those of the equilibrium algorithms.

In Section II, it was mentioned that the transverse shear stiffness matrix (22) causes maximizing sequences for the total strain energy which are of very slow convergence. This is because of the fact that, in (13), the contributions of rotations θ_x and θ_y vary linearly in the triangle, whereas those of w are constant. As the grid size gets smaller, only the contributions of average rotations remain, and those of linearly varying terms rapidly diminish. This suggests that, in (13), one may use average rotations in place of the total linear rotations field of the triangle. When implemented, this yields:

$$\{\gamma\} = \frac{1}{2A}[\mathbf{L} \,\vdots\, -\mathbf{I} \,\vdots\, \mathbf{J}] \begin{Bmatrix} \mathbf{w} \\ \hdashline \theta_x \\ \hdashline \theta_y \end{Bmatrix} \quad (46)$$

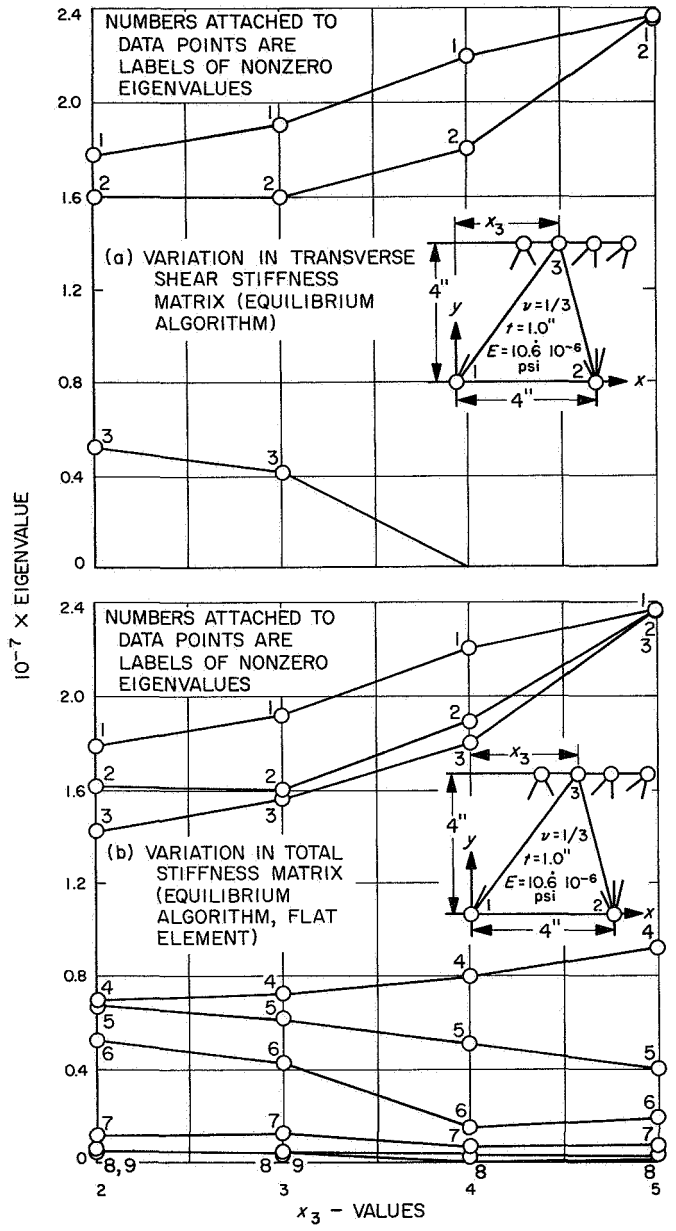

Fig. 13. Variation of eigenvalues with geometry, after constant trace scheme: (a) Transverse shear stiffness matrix (28); (b) Total stiffness matrix (36) ($x_0 = y_0 = z_0 = 0$)

where

$$[\mathbf{I}] = \frac{2A}{3}\begin{bmatrix} 0 & 0 & 0 \\ 1 & 1 & 1 \end{bmatrix}$$

$$[\mathbf{J}] = \frac{2A}{3}\begin{bmatrix} 1 & 1 & 1 \\ 0 & 0 & 0 \end{bmatrix}$$

Using (46) in (4) and differentiating yields

$$[\mathbf{K}_{S2}] = \frac{t}{4A}\left[\begin{array}{c|c|c|c|c} \mathbf{0} & \mathbf{0} & \mathbf{0} & \mathbf{0} & \mathbf{0} \\ \hline \mathbf{0} & \mathbf{0} & \mathbf{0} & \mathbf{0} & \mathbf{0} \\ \hline \mathbf{0} & \mathbf{0} & \mathbf{S}_{11} & \mathbf{Z}_{21}^T & \mathbf{Z}_{31}^T \\ \hline \mathbf{0} & \mathbf{0} & \mathbf{Z}_{21} & \mathbf{Z}_{22} & \mathbf{Z}_{32}^T \\ \hline \mathbf{0} & \mathbf{0} & \mathbf{Z}_{31} & \mathbf{Z}_{32} & \mathbf{Z}_{33} \end{array}\right] \tag{47}$$

where

$$[\mathbf{Z}_{21}] = -[\mathbf{I}^T][\mathbf{D}'][\mathbf{L}]$$
$$[\mathbf{Z}_{32}] = -[\mathbf{J}^T][\mathbf{D}'][\mathbf{I}]$$
$$[\mathbf{Z}_{31}] = [\mathbf{J}^T][\mathbf{D}'][\mathbf{L}]$$
$$[\mathbf{Z}_{33}] = [\mathbf{J}^T][\mathbf{D}'][\mathbf{J}]$$
$$[\mathbf{Z}_{22}] = [\mathbf{I}^T][\mathbf{D}'][\mathbf{L}]$$

In order to obtain the total stiffness matrix, one may use (47), (21), and (33) in (25).

$$[\mathbf{K}_4] = [\mathbf{K}_{M3}] + [\mathbf{K}_B] + [\mathbf{K}_{S2}] \tag{48}$$

Note that (33) is used as the membrane stiffness matrix to avoid the use of the equilibrium algorithm. Matrices (47) and (48) satisfy all equilibrium requirements.

Figures (14) and (15) show the behaviors of (47) and (48), respectively. As observed from these figures, $[\mathbf{K}_{S2}]$ and $[\mathbf{K}_4]$ are always positive and of rank 2 and 8, respectively.

V. Comparison of Methods of Improvement

In this section the methods of improvement proposed in the previous section are compared. First, to demonstrate the adverse effects of casual triangulation when (36) is used, a plate problem is solved with various triangulations. A clamped square plate 48 in. long and 1 in. thick and subjected to a central transverse concentrated load of 10 lb is taken. The plate material has a Young's modulus of 10.6×10^6 psi and a Poisson ratio of ⅓. Using the symmetry of the solution, only ⅛ of the plate is considered. On the middle plane of ⅛ plate, 28 nodes are used, 18 on the boundary and 10 inside. By keeping the locations of the boundary nodes constant, varying the locations of internal nodes, and randomly joining neighboring nodes, about 200 different triangulations are generated. The solution for each case is obtained by using (36) without any of the improvement schemes.

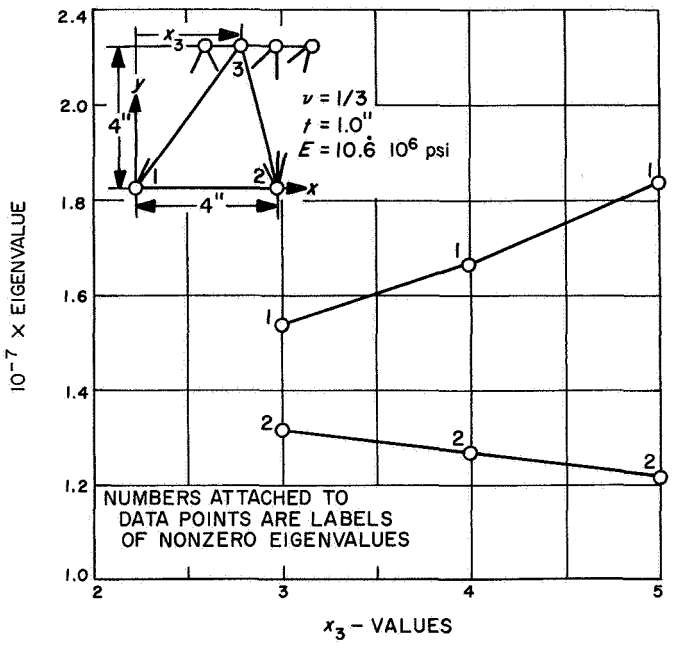

Fig. 14. Variation of eigenvalues of transverse shear stiffness matrix (47) with geometry

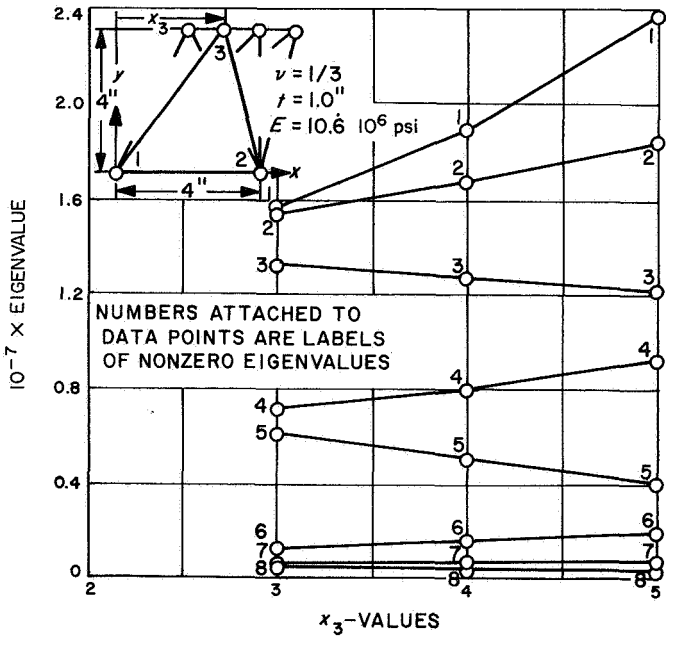

Figure. 15. Variation of eigenvalues of total stiffness matrix (48) with geometry ($x_0 = y_0 = z_0 = 0$)

It was observed that the deflections did not vary more than 5% unless there were more than two obtuse triangles in the system, in which case patently ridiculous results for a structural problem were obtained. Figure 16 shows two of these solutions and associated triangulations. Note that when obtuse triangles exist, the computed deflections

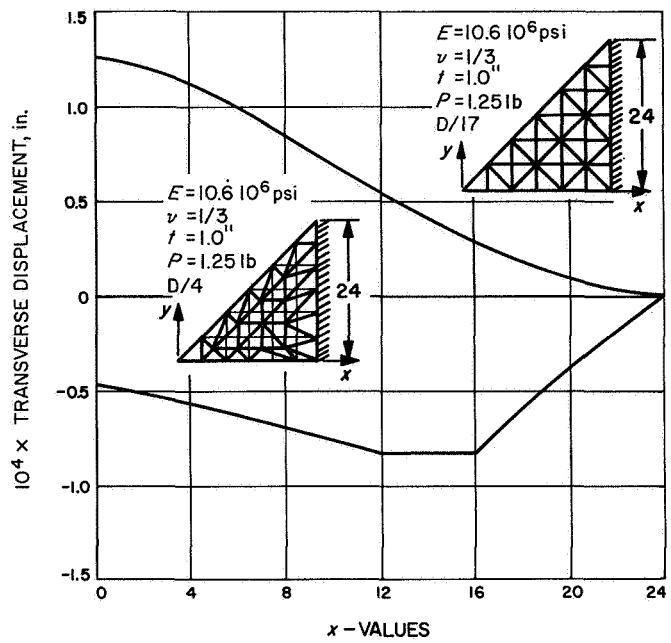

Fig. 16. Effect of triangulation on the solution by (36) (centrally loaded clamped square plate)

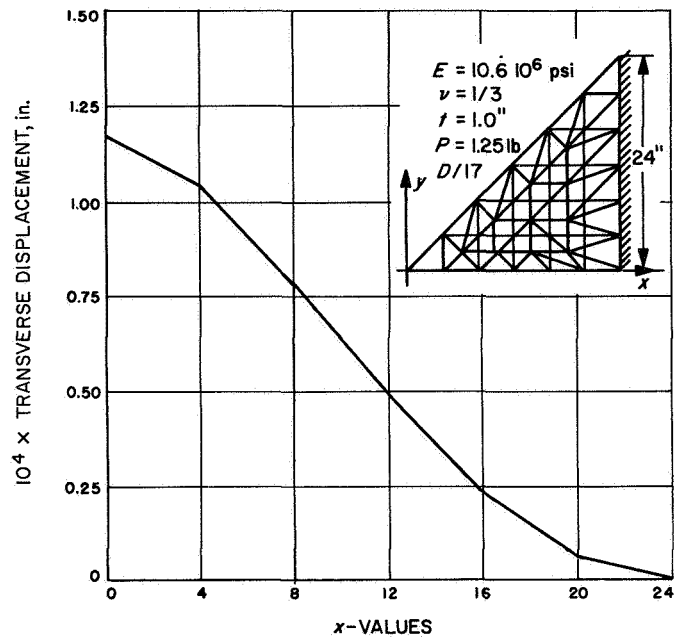

Fig. 17. Transverse displacements of centrally loaded clamped square plate along +x-axis, as obtained by using (36), after the absolute value scheme

are in opposite direction with the load, which is a concrete indication of nonpositive behavior.

Figures 17 and 18 show the transverse displacements obtained for the same case of obtuse triangulation, after the absolute value and the constant trace schemes, respectively. The improvement is obvious. A discussion as to which of the two schemes is better follows.

Comparing Figs. 12a and 13a, it may be observed that the spectrum width of eigenvalues is larger in the absolute value scheme than it is in the constant trace scheme. The same is observable in Figs. 12b and 13b. Since in the plate problem the bending modes are dominant, the behavior of small eigenvalues of the total stiffness matrix (associated with the bending modes as observed in Section III) is more important than the spectrum width. Comparison of Figs. 12b and 13b indicates that the bending eigenvalues of Fig. 13b are smaller and one less in number than those of Fig. 12b. Referring to (42), this observation implies that the constant trace scheme will yield larger deflections than the absolute value scheme. This conclusion is observable from Figs. 17 and 18.

In Fig. 19, a comparison is made of the convergence rates of maximizing sequences, as obtained by the equilibrium (36) and the average rotations (48) algorithms for the clamped plate problem. The triangulation of ⅛ plate is such that the nodes are uniformly distributed over the

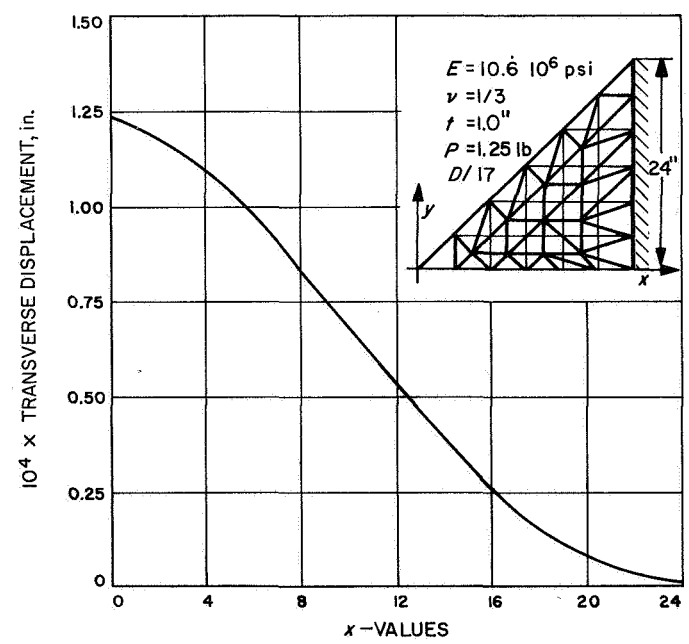

Fig. 18. Transverse displacements of centrally loaded clamped square plate along x-axis, as obtained by using (36), after the constant trace scheme

middle plane. This triangulation is used for both cases. Figure 19 shows that the average rotations algorithm, although theoretically more appealing, yields a maximizing sequence which is of much slower convergence than

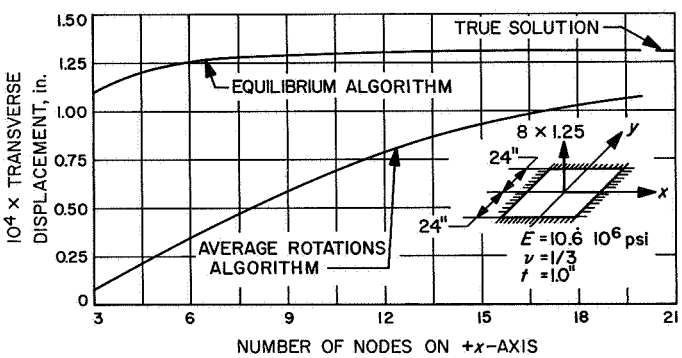

Fig. 19. Comparison of convergence rates of equilibrium and average rotations algorithms (central transverse displacement of centrally loaded clamped square plate)

that of the equilibrium algorithm. A discussion of this follows.

Comparing Figs. 13a and 14, one sees that the spectrum width of eigenvalues is smaller in (47) than in (28). The same is observable for (48) and (36) from Figs. 13b and 15, respectively. However, the bending eigenvalues of (36) are smaller than those of (48). This indicates that (28), when superimposed on (21), lowers the eigenvalues of (21). This coupling only weakly materializes when (47) is superimposed on (21). Referring to (42), this observation explains the slow convergence characteristics of (48).

VI. Suggested Matrix and Convergence Characteristics

In the previous sections, five representations—(25), (34), (35), (36), and (48)—and two improvement schemes are given for the triangular shell element. All these matrices satisfy the equilibrium requirements; they are symmetric and positive, and they are all geometry-insensitive if one of the improvement schemes is used.

The study in Section V indicates that the constant trace scheme is superior to the absolute value scheme, and the matrices generated with the help of equilibrium, i.e., (34), (35), and (36), have much better convergence characteristics than those generated without this help, i.e., (25) and (47). Matrix (25) is the worst one as far as convergence is concerned. Among these matrices, the one which may be obtained by (36) and the absolute value scheme is the matrix reported in Ref. (1).

Among the rapidly convergent representations, (36) is the easiest to generate. By avoiding obtuse triangles during the triangulation, this representation can be used directly without any of the improvement schemes.

A theoretically more appealing matrix for shells is probably the one given by (35), which may be used without any of the improvement schemes, provided that the obtuse triangles are avoided. However, (35) requires one more piece of data, z_0 than required by (36). The comparison of solutions with (35) and (36) indicated that not much is gained by taking the curvatures in the element.

Matrix (34) is probably the hardest to generate, since it requires three pieces of additional data (x_0, y_0, and z_0) and necessitates the use of one of the improvement schemes even if the triangulation avoids obtuse triangles.

The convergence characteristics of (36) without any improvement scheme is studied by using nonobtuse triangulation. The results are summarized in Figs. 20–23. In these figures the data points have been joined by straight lines. Figure 20 studies the convergence of the maximizing sequence in the clamped plate problem, which was described previously. In the triangulation, the nodes are uniformly distributed in the middle plane. As observed from the figure, the convergence is rapid and monotonic.

The convergence phenomenon is also studied in a clamped spherical cap for pressure loading in Fig. 21, and for a central transverse concentrated load in Figs. 22 and 23. Uniform grids were used for the cases presented in Figs. 21 and 22. The case presented in Fig. 23 uses a grid which gets uniformly coarser away from the concentrated force. The spherical cap problem was first solved for a 60-deg slice, assigning each node 3 degrees of freedom. Later, the condition that nodal deflections of a parallel are identical was imposed on the overall stiffness matrix before inversion, and the solution was completed for the same 60-deg slice. These two solutions indicated that the latter requires very short computer time and the results are not disturbed at all by the roundoff errors. The results presented in Figs. 21, 22, and 23 were obtained with the latter approach.

Since it is not readily observable from Fig. 21 that the sequence is maximizing, the concentrated load problem of Figs. 22 and 23 is included. Figure 21 merely indicates that the sequence is monotonically converging. On the other hand, Fig. 22 clearly indicates that the sequence is a maximizing one. (Note that the central transverse displacement in Figs. 22 or 23 is a measure of total strain energy, and it is monotonically increasing with grid refinement. This feature does not exist in the pressure problem of Fig. 21.) Figure 23 is included to show that nonuniform grids may be used advantageously for obtaining rapidly changing deflection fields.

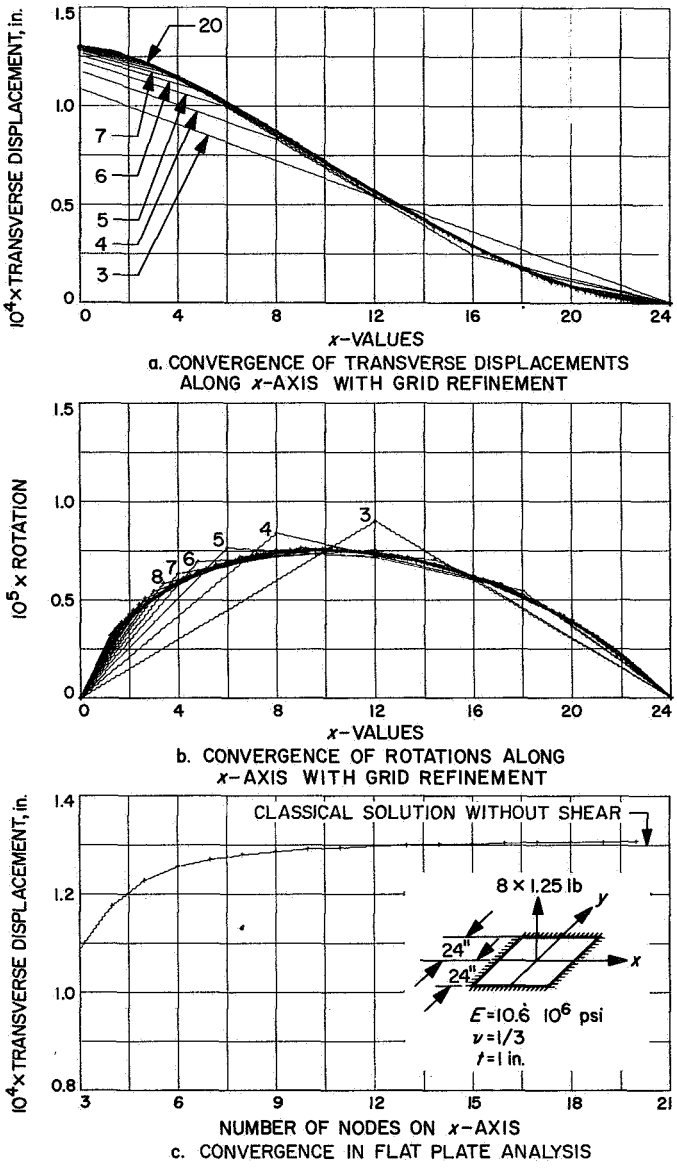

Fig. 20. *Clamped square plate subjected to a transverse concentrated force at center; solutions by (36); uniform grid (curve labels indicate the number of nodes on +x-axis)*

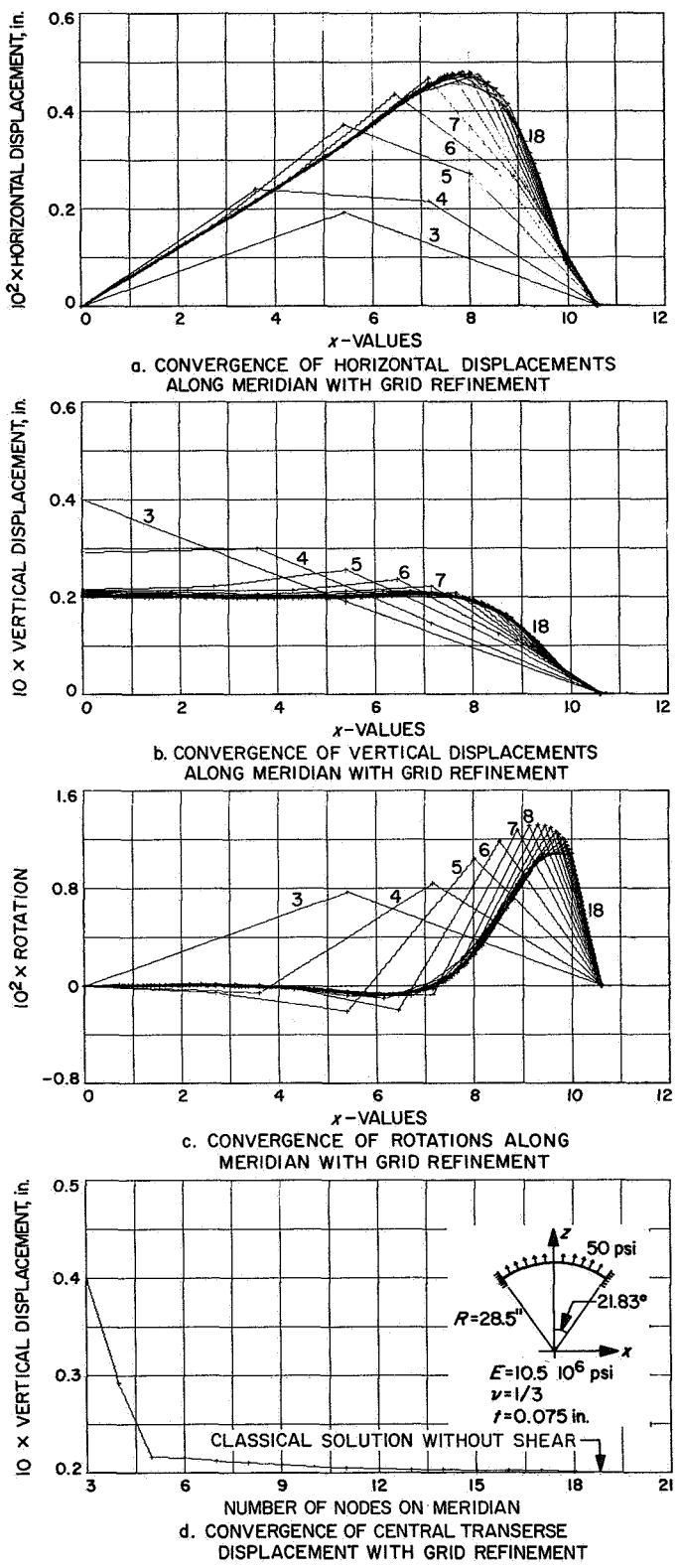

Fig. 21. Clamped spherical cap subjected to pressure loading; solution by (36); uniform grid (curve labels indicate the number of nodes on the meridian)

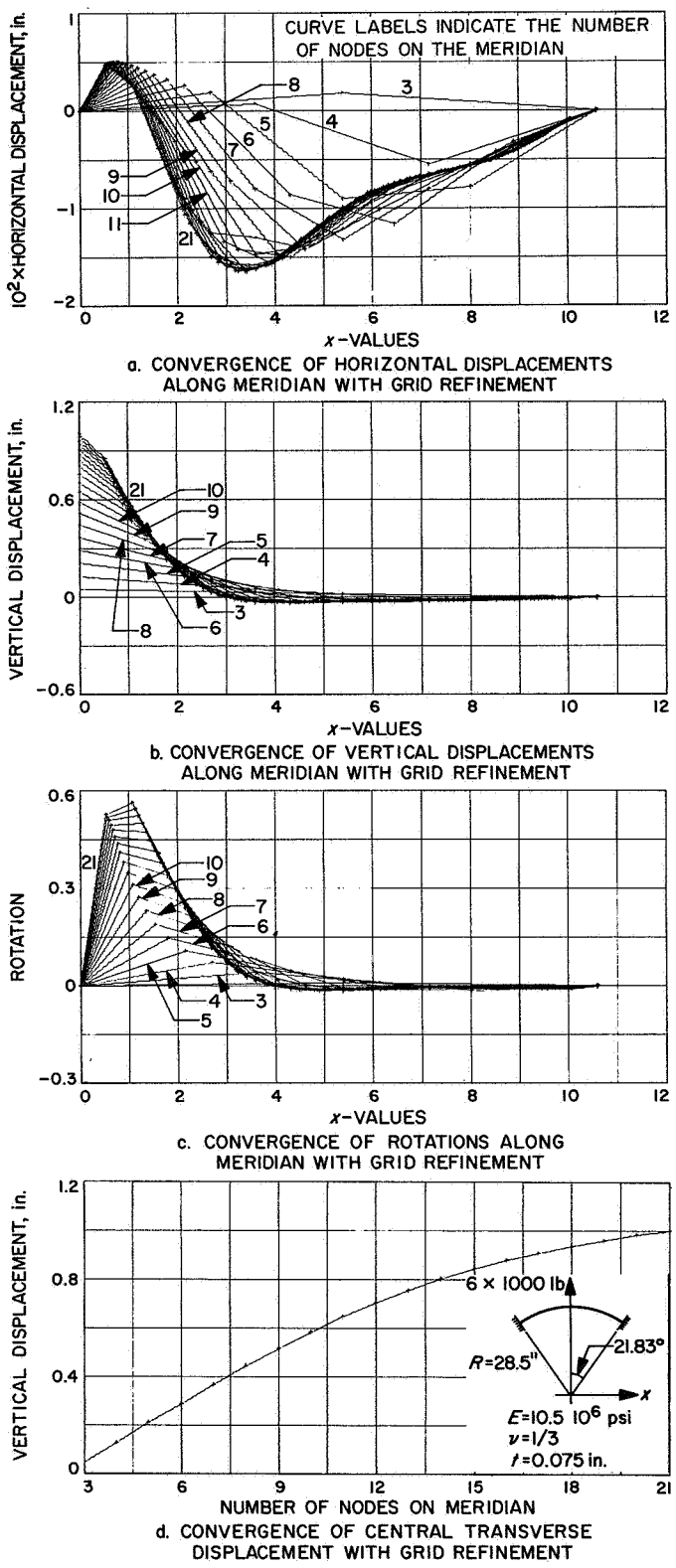

Fig. 22. Clamped spherical cap subjected to a transverse concentrated force at center; solutions by (36); uniform grid

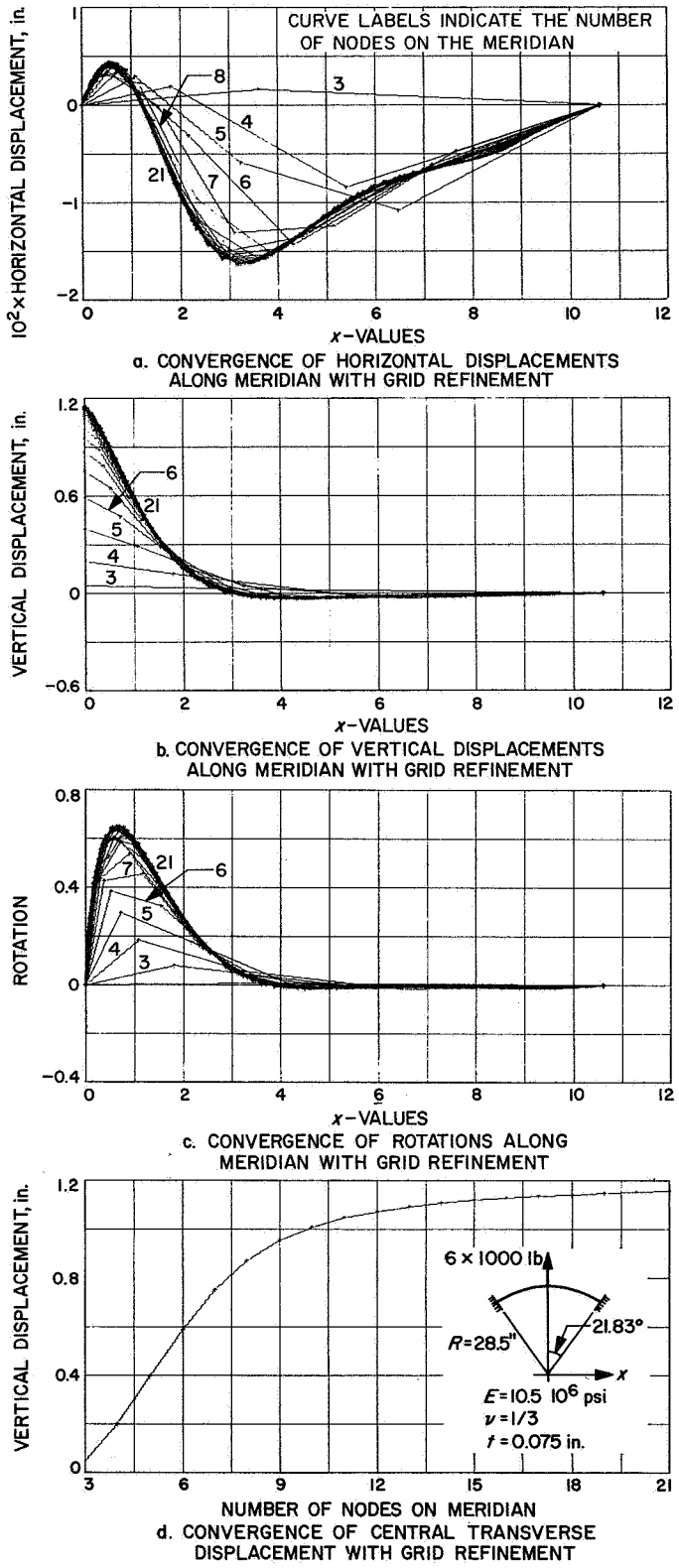

Fig. 23. Clamped spherical cap subjected to a transverse concentrated force at center; solutions by (36); grid gets monotonically coarser away from the force

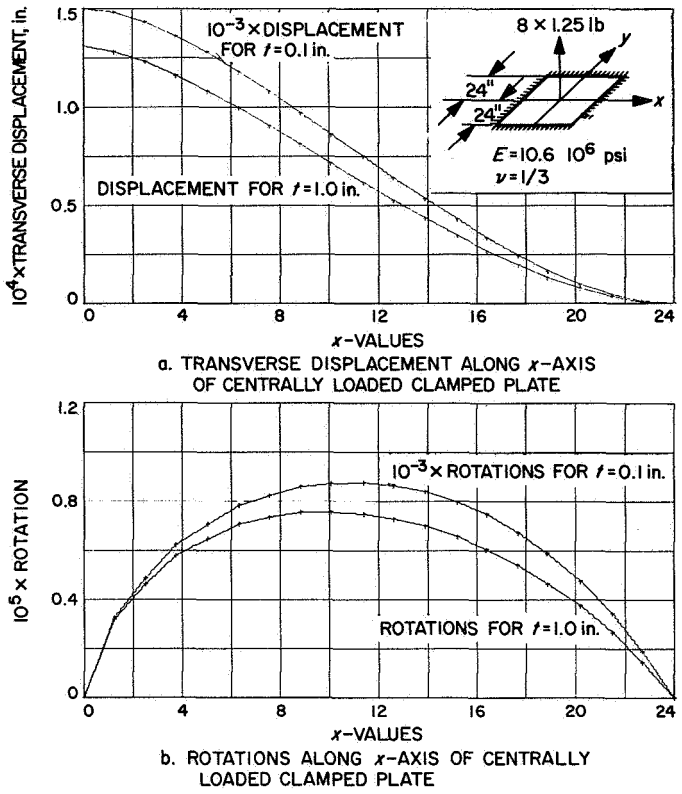

Fig. 24. Demonstration of the fact that deflections vary basically with thickness cubed; solutions by (36)

In Fig. 24, the effect of thickness/area ratio is studied in the clamped plate problem. For the same triangulation, the problem was solved once for $t=1$ in. and once for $t=0.1$ in. thickness. From the linear theory of plates, one knows that transverse displacement increases 1000 times when the thickness is decreased 10 times if the transverse shear deformations are not taken into account. The same behavior may be observed from Fig. 24, if one remembers that the transverse shear effects are not ignored.

VII. Analysis Guidelines

This section discusses some guidelines to be employed in laying out the gridwork when the triangular shell element is used in the analysis of a curved surface.

Because of the added approximation for obtuse angles, the analyst should avoid large-angle triangles. This can be easily achieved by the following rule. First, join the nodes to create a quadrilateral grid; then triangulate the quadrilaterals by the shortest diagonal. Using this rule, the obtuse triangle grid in Fig. 16 is reestablished in Fig. 25 without moving any of the nodes. Using (36) as it

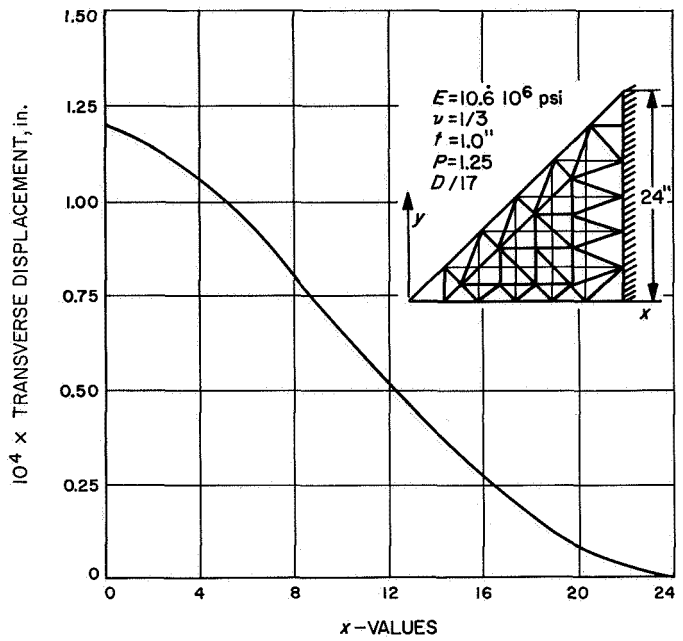

Fig. 25. Transverse displacements of centrally loaded clamped square plate; solution by (36); triangulation with shortest diagonal

is, the deflections for this latter grid are obtained. The transverse displacements are shown in Fig. 25. The advantage of triangulation with this rule is obvious from the comparison of Figs. 16 and 25.

The manner in which the analyst chooses to vary his node distribution will affect analysis accuracy. In general, the analyst should choose more nodes in regions of highly varying deflections. Figure 26 shows the dramatic improvement that can be obtained by using a nonuniform grid. This figure is produced by superimposing Figs. 22d

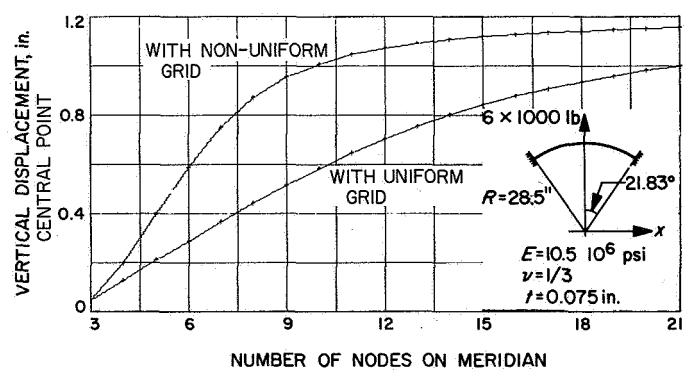

Fig. 26. Advantage of using smaller mesh size around the concentrated load for rapid convergence; solutions by (36)

and 23d. No attempt was made in the analysis presented in Fig. 23, to optimize the gridwork spacing. The figure does, however, demonstrate that the errors can be reduced by an order of magnitude by using irregular grids.

Whenever possible, the analyst should try to use equilateral triangles. This will minimize both the truncation and roundoff errors. As far as the roundoff errors are concerned, this conclusion is evident, based upon the criterion that matrix conditioning is a function of the ratio of the maximum to minimum (nonzero) eigenvalues of the matrix. For each representation studied, this ratio increases as the largest angle in the triangle is increased from 60 deg. As to the discretization errors, one may refer to Synge (Ref. 5).

During the analysis of the spherical cap under pressure (Fig. 21), a peculiar result was obtained when the convergence was examined with grid refinement. This result was determined to be caused by the inaccuracy of grid-point coordinates. Figure 27 shows the accuracy for the analyses for 4- and 7-digit grid-point coordinate accuracy. This result indicates that if successive refinement is used for extrapolation, the analyst must exercise care in defining his structural geometry to ensure the validity of extrapolation.

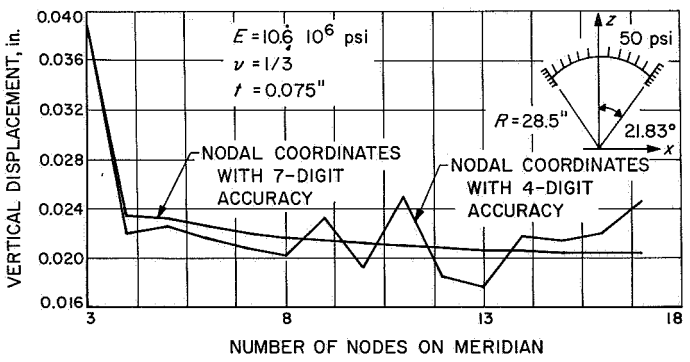

Fig. 27. Effect of accuracy in nodal coordinates on the solution; variation of central transverse displacement with grid refinement in clamped spherical cap subjected to pressure; solutions by (36)

VIII. How the Curvatures Are Accounted For

In Section VI, it was mentioned that the curvatures in the element contribute very little to the computed deflections. Actually, the cases presented in Figs. 21, 22, and 23 were first analyzed (Ref. 2) with (35). The results of these analyses, when compared with those presented in Figs. 21, 22, and 23, verify this statement. As discussed in Section II, the contribution of curvatures in the element is proportional to (grid-size/radius-of-curvature) ratio, which diminishes rapidly with grid refinement. Figure 27 verifies that the curvatures are actually accounted for by the differences in the orientations of the neighboring elements. The increasing oscillations in the 4-digit accuracy solution show that, when the nodes are too close to each other, the curvatures (quantities related with the second differences of nodal coordinates) require higher accuracy in the nodal coordinates if (37) is to be used before the assembly. This difficulty may be eliminated by expressing (37) directly in terms of the curvatures provided at the nodes. This task is outside of the scope of this paper.

IX. Summary of Significant Developments

The developments presented herein are summarized as follows:

(1) The derivation of several stiffness matrices for triangular shell element is reviewed.

(2) By studying the eigenvalues, it is shown that stiffness matrices produced with the help of equilibrium requirements may display nonpositive behavior. The grave consequences of nonpositive behavior are demonstrated.

(3) Two schemes (one of which was proposed by Melosh (Ref. 1) previously) are presented to correct the nonpositive behavior.

(4) It is demonstrated that the equilibrium algorithm can be used to accelerate the convergence.

(5) The fact is demonstrated that the stiffness matrices associated with polyhedral deflection fields produce maximizing sequences for the total strain energy with grid refinement.

(6) It is shown that the curvatures in the element contribute very little to the computed deflections, even in the reasonably crude grids.

(7) The effect of thickness/area ratio is demonstrated.

(8) Guidelines are presented for the use of triangular shell element in structural analyses.

(9) The way that the curvatures are taken into account is discussed.

Results presented in Figs. 16–27 were obtained by means of the ELAS general purpose program of the Jet Propulsion Laboratory.

References

1. Melosh, R. J., "A Flat Triangular Shell Element Stiffness Matrix," AFFDL-TR-66, Air Force Flight Dynamics Laboratory, Wright-Patterson AFB, Ohio, October 26–28, 1966, pp. 503–509.

2. Utku, S.,"Stiffness Matrices for Thin Triangular Elements of Non-Zero Gaussian Curvature," *AIAA J.*, Vol. 5, No. 9, pp. 1650–1657, September 1967.

3. Marguerre, K., "Zur Theorie der gekrummten Platte grosser Formänderung," *Proceedings of the Fifth International Congress of Applied Mechanics,* Cambridge, Mass., 1938, pp. 93–101.

4. Prager, W., and Synge, J. L., "Approximations in Elasticity Based on the Concept of Function Space," *Quart. Appl. Math.*, Vol. 5, 1947, pp. 241–269.

5. Synge, J. L., *The Hypercircle in Mathematical Physics,* Cambridge University Press, Cambridge, England, 1957, pp. 209–213.